Redox Biology 72 (2024) 103145

Contents lists available at ScienceDirect

Redox Biology

journal homepage: www.elsevier.com/locate/redox

The positive feedback loop of the NAT10/Mybbp1a/p53 axis promotes cardiomyocyte ferroptosis to exacerbate cardiac I/R injury

Zhezhe Qu [a,1], Xiaochen Pang [a,1], Zhongting Mei [a], Ying Li [a], Yaozhi Zhang [a], Chuanhao Huang [a], Kuiwu Liu [a], Shuting Yu [a], Changhao Wang [a], Zhiyong Sun [a], Yingqi Liu [a], Xin Li [a], Yingqiong Jia [a], Yuechao Dong [a], Meixi Lu [e], Tiantian Ju [a], Fan Wu [a], Min Huang [a], Na Li [a], Shunkang Dou [a], Jianhao Jiang [a], Xianhui Dong [a], Yi Zhang [a], Wanhong Li [a], Baofeng Yang [a,b,c,*], Weijie Du [a,b,c,d,*]

[a] State Key Laboratory of Frigid Zone Cardiovascular Diseases (SKLFZCD), Department of Pharmacology (State-Province Key Laboratories of Biomedicine-Pharmaceutics of China, Key Laboratory of Cardiovascular Research, Ministry of Education), College of Pharmacy, Harbin Medical University, Harbin, China
[b] Northern Translational Medicine Research and Cooperation Center, Heilongjiang Academy of Medical Sciences, Harbin Medical University, Harbin, China
[c] Research Unit of Noninfectious Chronic Diseases in Frigid Zone, Chinese Academy of Medical Sciences, 2019RU070, Harbin, China
[d] Eye Hospital, The First Affiliated Hospital of Harbin Medical University, Harbin, Heilongjiang Province, China
[e] Traditional Chinese Medicine School, Beijing University of Chinese Medicine, Beijing, China

ARTICLE INFO

Keywords:
NAT10
ac4C
I/R injury
p53
Mybbp1a
Ferroptosis

ABSTRACT

Ferroptosis is a nonapoptotic form of regulated cell death that has been reported to play a central role in cardiac ischemia–reperfusion (I/R) injury. N-acetyltransferase 10 (NAT10) contributes to cardiomyocyte apoptosis by functioning as an RNA ac4c acetyltransferase, but its role in cardiomyocyte ferroptosis during I/R injury has not been determined. This study aimed to elucidate the role of NAT10 in cardiac ferroptosis as well as the underlying mechanism. The mRNA and protein levels of NAT10 were increased in mouse hearts after I/R and in cardiomyocytes that were exposed to hypoxia/reoxygenation. P53 acted as an endogenous activator of NAT10 during I/R in a transcription-dependent manner. Cardiac overexpression of NAT10 caused cardiomyocyte ferroptosis to exacerbate I/R injury, while cardiomyocyte-specific knockout of NAT10 or pharmacological inhibition of NAT10 with Remodelin had the opposite effects. The inhibition of cardiomyocyte ferroptosis by Fer-1 exerted superior cardioprotective effects against the NAT10-induced exacerbation of post-I/R cardiac damage than the inhibition of apoptosis by emricasan. Mechanistically, NAT10 induced the ac4C modification of Mybbp1a, increasing its stability, which in turn activated p53 and subsequently repressed the transcription of the anti-ferroptotic gene SLC7A11. Moreover, knockdown of Mybbp1a partially abolished the detrimental effects of NAT10 overexpression on cardiomyocyte ferroptosis and cardiac I/R injury. Collectively, our study revealed that p53 and NAT10 interdependently cooperate to form a positive feedback loop that promotes cardiomyocyte ferroptosis to exacerbate cardiac I/R injury, suggesting that targeting the NAT10/Mybbp1a/p53 axis may be a novel approach for treating cardiac I/R.

1. Introduction

Acute myocardial infarction (AMI) is a leading cause of morbidity and mortality worldwide [1,2]. Timely reperfusion of coronary blood is the most effective therapeutic approach for limiting MI and preserving cardiac function in patients with AMI. However, reperfusion can often exacerbate cardiac damage; this phenomenon is referred to as ischemia–reperfusion (I/R) injury. Although considerable efforts have been made to explore the underlying molecular mechanism involved, feasible therapeutic targets for clinically attenuating cardiac I/R injury are still lacking.

* Corresponding authors. State Key Laboratory of Frigid Zone Cardiovascular Diseases (SKLFZCD), Department of Pharmacology (State-Province Key Laboratories of Biomedicine-Pharmaceutics of China, Key Laboratory of Cardiovascular Research, Ministry of Education), College of Pharmacy, Harbin Medical University, Harbin, China.
E-mail addresses: yangbf@ems.hrbmu.edu.cn (B. Yang), duweijie@hrbmu.edu.cn (W. Du).
[1] These authors contributed equally to this work.

https://doi.org/10.1016/j.redox.2024.103145
Received 15 February 2024; Received in revised form 28 March 2024; Accepted 30 March 2024
Available online 2 April 2024
2213-2317/© 2024 The Authors. Published by Elsevier B.V. This is an open access article under the CC BY-NC license (http://creativecommons.org/licenses/by-nc/4.0/).

Abbreviation

I/R	Ischemia Reperfusion
H/R	hypoxia/reoxygenation
NAT10	N-acetyltransferase 10
ac4C	N4-acetylcytidine
NMCMs	Primary neonatal mouse cardiomyocytes
Fer-1	Ferrostatin-1
Emr	Emricasan
LDH	Lactate dehydrogenase activity
CKMB	Creatine Kinase Isownzyme-MB
MB	Methylene Blue
LPO	Lipid peroxidation
MDA	Malondialdehyde
EF	Ejection Fraction
FS	Fractional Shortening
Mybbp1a	MYB binding protein 1A

Ferroptosis, which is different from apoptosis, necrosis and autophagy, is a type of iron-dependent programmed cell death that is characterized by the excessive lipid peroxidation due to redox imbalances. Ferroptosis has been well accepted as a key driver of cardiac impairment after MI [3–6]. A recent study demonstrated that apoptosis occurs during the early phase of I/R (within 4 h), while ferroptosis is the major type of cell death that occurs during the late phase of I/R (especially 24 h to 7 days) [3]; additionally, inhibition of ferroptosis results in superior protection against cardiac I/R injury compared with prevention of other types of cell death [3,7,8]. Solute carrier family 7 member 11 (SLC7A11) is a key suppresser of ferroptosis that is responsible for transporting extracellular cystine into the cell in exchange for glutamate. The intracellular cystine is converted to glutathione, which is utilized by the antioxidant enzyme glutathione peroxidase 4 (GPX4) to decrease the accumulation of lipid peroxides, thereby inhibiting ferroptosis. P53 is a transcription factor that initiates several types of cell death, including ferroptosis [9,10]. The acetylation of p53 that occurs in response to cellular stress is indispensable for p53 stability and transcriptional activity. Under oxidative stress, acetylation of p53 in its carboxyl-terminal region (CTD) facilitates cell ferroptosis via the transcriptional repression of SLC7A11 [9,11].

The nucleolar N-acetyltransferase 10 (NAT10) protein is a member of the GCN5-related N-acetyltransferase family of HATs, and it was initially shown to participate in many pathophysiological processes by catalyzing specific substrates via its acetyltransferase activity [12]. In addition, NAT10 can function as an RNA acetyltransferase by mediating the acetylation of tRNAs, rRNAs and mRNAs. NAT10-catalyzed N4-acetylcytidine (ac4C) acetylation of mRNA has been shown to increase mRNA stability and translational efficiency [13]. Recent studies have reported that NAT10 participates in cardiomyocyte apoptosis and cardiac remodeling in response to different stimuli [14,15]. However, the changes in and role of NAT10 in I/R-induced ferroptosis remain to be determined.

MYB-binding protein 1A (Mybbp1a) was initially identified as a partner that interacts with proteins encoded by the proto-oncogene c-MYB [16]. It has been shown that Mybbp1a mediates diverse biological processes by interacting with many transcription factors [17–19]. Mybbp1a is predominantly localized in the nucleolus and translocates into the nucleoplasm when the nucleolar structure is disrupted upon DNA damage [20]. Mybbp1a then directly binds to lysine residues in the CTD of p53 and triggers p53 tetramerization. Moreover, Mybbp1a recruits p300 to facilitate p53 acetylation, which leads to increased p53 stability and transcriptional activity [21,22]. However, whether Mybbp1a participates in the pathogenesis of cardiac diseases has not been determined.

In this study, we found that the I/R-induced upregulation of NAT10 is regulated by p53 in a transcription-dependent manner. Using gain- and loss-of-function strategies, we identified the pro-ferroptotic effect of NAT10 as the main trigger of cardiac I/R injury. NAT10 enhanced the stabilization of Mybbp1a by causing the ac4C modification of its mRNA, thereby resulting in the activation of p53 and subsequently repressing the transcription of the anti-ferroptotic gene SLC7A11. These findings suggest that targeting the NAT10/Mybbp1a/p53 axis is a promising novel direction for treating cardiac I/R injury.

2. Materials and methods

2.1. Animals

Neonatal C57BL/6 mice were obtained from the Laboratory Animal Center of the Second Hospital of Harbin Medical University. Approximately 10-week-old male C57BL/6 mice weighing 18–22 g were provided by Changsheng Bio-Technology (Liaoning, China). Mice were housed in a facility with a room temperature of 23 ± 2°C and a humidity of 55 ± 5%. The air exchange rate is 10–15 times/hour with fresh air, and 12 h of alternating light is maintained every day. All animal procedures conformed to the Guide for the Care and Use of Laboratory Animals published by the U.S. National Institutes of Health and were approved by the Animal Ethical Committee of Harbin Medical University (NO. IRB3007822).

2.2. Construction and generation of cardiomyocyte-specific NAT10 knockout mice

Cardiomyocyte-specific NAT10 knockout mice were generated by Cyagen Biosciences Inc (Guangzhou, China). Using the principle of Cre/loxP recombination system, conditional knockout was performed to produce myocardial tissue-specific NAT10 knockout mice. $NAT10^{f/f}$ mice were constructed by inserting two loxP sites at both ends of the fourth exon of NAT10 gene. $NAT10^{f/f}$ mice were obtained by self-crossing. $NAT10^{f/+}$/Myh6-Cre mice were obtained by crossing Myh6-Cre mice with $NAT10^{f/f}$ mice for one generation. The genotypes of NAT10 knockout mice were identified by PCR. Western blotting was used to identify the knockout efficiency of $NAT10^{f/+/Myh6-Cre}$ mice. Primers for targeted allele and Myh6-Cre transgene are in Supplementary Table 1.

2.3. Mouse model of cardiac I/R injury

I/R injury in mice was induced by 45-min ischemia, followed by 24-h reperfusion. In brief, mice were anesthetized with 2% avertin (0.1 mL/10g body weight; Sigma-Aldrich Corporation, United States) by intraperitoneal injection. Then the mice underwent endotracheal intubation and the left anterior descending coronary artery (LAD) was ligated with 7-0 nylon for 45 min. Mice were anesthetized after 24-h reperfusion for assessing heart function by echocardiographic measurement. Mice were euthanized and tissue samples from the ischemic area were harvested and stored at −80°C for further assays.

2.4. Neonatal mouse cardiomyocytes (NMCMs) preparation and culture

Neonatal mouse cardiomyocytes (NMCMs) were isolated from 1- to 3-day-old mice. Briefly, after rinsed in the PBS, the isolated hearts of neonatal mice were cut into pieces and digested in trypsin-EDTA solution. (Trypsin 0.25%, EDTA 0.53 Mm, Beijing Solarbio Science & Technology Co., Ltd., China). The obtained cells were cultured in Dulbecco's modified Eagle medium (DMEM, Gibco, USA) supplemented with 10% fetal bovine serum (10%FBS, South America), 1% 10 KU/mL Penicillin G Sodium salt/10 mg/mL Streptomycin Sulfate (meilunbio, Liaoning, China). After adherent culture of the cell mixture in a 37°C incubator with 5% CO_2 for 90 min, the suspended cardiomyocytes were

transferred to a six-well culture plate at a density of 1×10^6 cells per well. The next experiment was performed after continued adherent culture for 48 h. NMCMs incubated under hypoxic condition (37°C with a humid atmosphere of 5% CO_2 and 1% O_2) for 12 h and followed by a 24-h reoxygenation to establish in vitro H/R model.

2.5. Infection of adeno-associated virus

The construction of adeno-associated serotype 9 (AAV9) virus vector using the interference sequence of NAT10 gene (AAV9-shNAT10) and Mybbp1a gene (AAV9-shMybbp1a) were designed and synthesized by Hanbio Biotechnology Co., Ltd (Shanghai, China). The construction of adeno-associated virus vector overexpressing NAT10 gene (AAV9-NAT10) was designed and synthesized by Genechem (Shanghai, China). The adeno-associated virus vector carrying NAT10, shNAT10, shMybbp1a and empty vector (1.5×10^{11} Vg/mL) were injected into the tail vein of mice (Diluted with 0.9% saline, 0.2 mL/animal). Cardiac I/R model was established three weeks later.

2.6. Echocardiographic measurements

Left ventricular (LV) function was assessed by a Vevo2100 echocardiographic system (VisualSonics, Toronto, ON, Canada) at a probe frequency of 10 MHz with M-mode recording. Mice were anesthetized with avertin and depilated with depilating cream on the chest. The limbs of mice were attached to heating pads to maintain body temperature at 37 °C. Medical ultrasound gel (Tianjin Yajie Medical Material Co. Ltd., Tianjin, China) was used as a coupling agent between the ultrasound scan-head and the skin. Left ventricular parameters such as left ventricular end-diastolic volume (LVEDV), left ventricular end-systolic volume (LVESV), left ventricular end-diastolic diameter (LVID; d) and left ventricular systolic diameter (LVID; s) were measured by M-mode recording. The data are presented as the average of measurements of three consecutive beats. Ejection fraction (EF) was calculated as EF = (LVEDV-LVESV)/LVEDV × 100% and fractional shortening (FS) was calculated as FS=(LVID; d-LVID; s)/LVID; d × 100%, respectively.

2.7. Evans blue/Triphenyl tetrazolium choride (TTC) double staining

At the end of the reperfusion phase, Evans blue/TTC double staining was performed to area at risk (AAR) and infarct area (IF). Specifically, the mice were anesthetized and the chest cavity was re-opened. The original location was ligated to re-close the LAD, 0.5 mL 2% Evans blue (Solarbio, China) was injected into the left ventricular cavity. The heart was quickly removed and washed in pre-cooled PBS. After freezing at −80 °C for 5 min, the ligature was cut into 4 pieces on average from the apex of the heart. After that, the slices were placed in 2% TTC (2,3, 5-triphenyltetrazonium chloride; Solarbio, China) solution and incubated at 37 °C for 5 min to observe infarct and viable myocardia. The slices were fixed in 4% paraformaldehyde for 30 min and then photographed. The non-ischemic area (blue staining), area at risk (AAR without Evans blue staining) including viable myocardium (red staining) and the infarct area (IF, light white staining) of each group of mice were determined by computer plane measurement, and the continuous sections of mice in each group were analyzed by Image Pro Plus software.

2.8. Lactate dehydrogenase (LDH) detection assay

Lactate dehydrogenase (LDH) was measured in serum from mice treated with different treatments using a lactate dehydrogenase assay kit (Nanjing Jiancheng, Jiangsu, China) according to the manufacturer's instructions and quantified with absorbance at 450 nm on a microplate reader (Bio Tek, Richmond, VA, USA).

2.9. Creatine Kinase MB Isoenzyme (CKMB) detection

The mice serum Creatine Kinase MB Isoenzyme (CKMB) was detected by using the mouse CKMB Elisa Kit (Elabscience, Wuhan, China) and quantified with absorbance at 450 nm on a microplate reader (Bio Tek, Richmond, VA, USA). Standard curves were fitted with Origin.

2.10. Adult mouse cardiomyocytes isolation

The heart was quickly removed and the aorta was cannulated on a constant-flow Langendorff instrument. Tyrode's (0.02 mg/mL) and bovine serum albumin (BSA; 1 mg/mL) to digest the heart. Tyrode's solution (mM) contained: NaCl 123, KCl 5.4, HEPES 10, NaH_2PO_4 0.33, $MgCl_2$ 1.0 and glucose 10; The pH was adjusted to 7.4 with NaOH. After tissue softening, the left ventricle was excised, lightly minced into small pieces, and then equilibrated in Tyrode solution of 200 μM $CaCl_2$ and 1% BSA. The cell suspension was filtered through a 100-mesh filter, and the cells in the filtrate were cardiomyocytes. Under the microscope, it is a long rod or rectangle, with clear stripes and sharp angles. There are cells in the visual field that can spontaneously contract.

2.11. Synthesis and transfection of overexpression plasmids and siRNAs

The siRNA of NAT10, Mybbp1a, p53 and a negative control was designed by Ribobio (Guangzhou, China). P53 plasmids were constructed by Genechem (Shanghai, China). Opti-MEM (Gibco, USA) was used to dilute X-treme GENE siRNA Transfection Reagent (Roche, Mannheim, Germany) and si-RNA, respectively. After 5 min, the two were mixed, and the mixture was added to serum-free cell culture medium 20 min later. Lipofectamine 2000 reagent (Invitrogen, Carlsbad, CA, USA) was used to transfect plasmids into cells in the same way. The sequences of siRNAs for mouse are in Supplementary Table 2.

2.12. Adenovirus construction

NAT10-carrying adenovirus for overexpression (Adv-NAT10) and empty vector-carrying adenovirus (Adv-Null) were constructed by Shanghai Hanbio Biotechnology Co., Ltd (Shanghai, China). Cardiomyocytes were infected with NAT10 adenovirus at a titer of 1×10^7 PFU/mL for 4 h, and 1 mL culture medium was added for another 2 h. Cells were collected for subsequent experiments after 48 h.

2.13. Inhibitor treatment

The clarified DMSO reserve liquid of 100 μL 25.0 mg/mL was added to 400 μL PEG300 and mixed evenly. 50 μL Tween-80 was added to the system and mixed evenly. Then continue to add 450 μL normal saline volume to 1 mL. According to the above system, 8 mL solvent was prepared and 2 mg Ferrostatin-1 (Fer-1, MedChemexpress, USA) powder was dissolved into it. Mice were given intraperitoneal injection of Fer-1 at 1 mg/kg/day the day before and after I/R surgery. According to the above system, 8 mL solvent was prepared and 5 mg Emricasan (Emr, MedChemexpress, USA) powder was dissolved into it. Mice were given intraperitoneal injection of Emr at 2.5 mg/kg/day the day before and after I/R surgery. An equal amount of solvent was injected intraperitoneally as a control.

Remodelin (selleck, USA) was dissolved in 0.5% sodium carboxymethyl cellulose (CMC-Na) solution. Mice were given 100 μL 0.5% CMC-Na solution or isometric Remodelin solution 100 mg/kg by gavage alone for 7 days, followed by I/R treatment. DMSO was added to the Remodelin powder to prepare a reserve solution with a concentration of 50 mM. Store at −80°C away from light. In the in vitro experiment, Remodelin reserve solution was added to the cell culture solution, making it a working solution with a final concentration of 40 μM, and the response of cardiomyocytes to the Remodelin was tested 24 h later.

2.14. RNA ac4C dot blot

The total RNA was isolated and immediately placed on ice. The total RNA dots were spotted onto a nylon membrane for purplish linkage. The membranes were washed in deionized water for 5 min and stained with methylene blue. Take a picture after a clear blue dot appears. Block with 5% milk for 1 h and incubate with ac4C antibody (ab253039 1:1000, abcam, Cambridge, United Kingdom) overnight at 4°C. The membranes were then washed three times for 5 min in 1*PBS/0.05% v/v Tween-20 (Sigma) and incubated with either horseradish-peroxidase-conjugated anti-rabbit IgG (1:5000, Beijing ZSGB-Bio). The luminescence signal was acquired and processed with a ChemiDoc MP (Bio-Rad).

2.15. Quantitative real-time PCR

Total RNA was extracted from collected cells or tissues by using TRIzol reagent (Invitrogen, Carlsbad, CA, United States). NANO-Drop2000c (Thermo Scientific, Carlsbad, USA) was utilized to verify the quality of RNA samples. Total RNA (500 ng) was reverse transcribed into cDNA using ReverTra Ace qPCR RT Kit (Toyobo Co., LTD, Japan). The ABI 7500 fast Real-Time PCR system (Applied Biosystems, Foster City, USA) was used to measure the expression levels of mRNAs by using SYBR Green (Toyobo Co., LTD, Japan). PCR amplification was performed as follows: 95°C for 10 min and 40 cycles at 95°C for 15 s, 60°C for 30 s, and 72°C for 30 s. β-actin and GAPDH were used as an internal control. The relative quantitative expression was determined using the $2^{-\Delta\Delta CT}$ method. All primers used in this study were in Supplementary Table 3.

2.16. Western blot

Total protein was isolated from cardiomyocytes and myocardium using RIPA lysis buffer (Beyotime, Shanghai, China). The total protein concentration was detected by a BCA Protein Assay Kit (Beyotime, Shanghai, China). Protein lysates were separated on 12% (vol/vol) SDS polyacrylamide gels and then transferred to nitrocellulose membranes (Millipore, Bedford, MA, USA) for subsequent studies. The membrane was blocked with 5% skim milk for 2 h and incubated with primary antibody at 4°C overnight. The secondary anti-rabbit or anti-mouse (LI-COR,Lincoln, USA) polyclonal antibody was used to conjugate the membrane at room temperature in dark for 60 min. An Odyssey infrared imaging system (LI-COR, Lincoln, NE, United States) was used to quantify the band intensity and measure the gray value and the relative level of protein was analyzed with Image Studio software. The primary antibodies were used in this study were in Supplementary Table 4.

2.17. Transmission electron microscopy (TEM)

The cells were collected and fixed by 2.5% glutaraldehyde. After being washed in 0.1 M sodium cacodylate buffer, cells were postfixed with 1% buffered osmium. The cells were dehydrated through the graded alcohol and embedded in resin. After dehydration through graded alcohol and embedding in resin, cells were incubated in a 60 °C oven for 3 days. Ultrathin sections were prepared and stained with uranyl acetate-lead citrate double staining, subsequently examined by a transmission electron microscope.

2.18. Immunohistochemistry (IHC) staining

Mice were euthanized and the hearts were perfused with saline through the left ventricle. Cardiac tissue was washed with PBS, fixed with 4% (w/v) paraformaldehyde for 24 h, and paraffin embedded. The paraffin sections were cut continuously with a thickness of 5 μm. The paraffin sections were roasted at 60°C for 2 h and then dewaxed. The degummed sections were incubated with 10 mM citrate buffer for antigen extraction. After endogenous peroxidase was blocked with 3% hydrogen peroxide at room temperature for 10 min, heart sections were incubated with a primary antibody against 4-HNE (bs6313R, Bioss, China) at 4°C overnight. Goat anti-Rabbit IgG/HRP (PV6001, Golden-Bridge, China) was then incubated at room temperature for 20 min as a secondary antibody. Then, 3, 3-diaminobenzidine (DAB) staining, hematoxylin reverse staining, neutral rubber seal. Images were captured under a fluorescence microscope (Olympus).

2.19. Lipid-peroxidation detection

Tissue blocks of equal size were added to 0.9% normal saline at 1:9 (g/L) and ground into tissue homogenate by ice bath. After 30 min of standing, the supernatant was centrifuged and used for lipid-peroxidation (Nanjing Jiancheng, Jiangsu, China) assessment according to the manufacturer's instructions and quantified with absorbance at 586 nm on a microplate reader (Bio Tek, Richmond, VA, USA).

Lipid-ROS level in cells was measured using the Image-iT® Lipid Peroxidation Kit (C10445, ThermoFisher Scientific, USA) according to the manufacturer's protocols. Cardiomyocytes were inoculated in 24-well plates and incubated with 5 μm C11 BODIPY at 37°C for 20 min. The image was obtained by fluorescence microscope (Olympus). Oxidized cell membranes show green fluorescence and non-oxidized cell membranes show red fluorescence.

2.20. Acetylated RNA immunoprecipitation (Ac-RIP)

Acetylated RNA immunoprecipitation (Ac-RIP) was performed using a Magna RIP RNA-Binding Protein Immunoprecipitation Kit (Millipore, Darmstadt, Germany). RNA was collected by adding RIP lysis buffer according to the manufacturer's instructions and incubated with anti-ac4C antibody (ab253039, 1:50, abcam, Cambridge, United Kingdom) and anti-IgG antibody (ab172730, 1:50, abcam, Cambridge, United Kingdom). After washing, RNA was precipitated with protein G magnetic beads. Ac4C modified RNA was extracted for quantitative analysis. PCR and agarose gel electrophoresis were performed to quantify the expression of RNAs.

2.21. Ac4C RIP-seq

RNA acetylation sequencing services are provided by CloudSeq Inc. (Shanghai, China). The ac4C-IP reaction was performed using GenSeq's RNA acetylation kit. The procedure was described as follows: Total RNA was extracted from the hearts of Sham and I/R mice, and the RNA was randomly fragmented into about 200 nt fragments. Protein A/G magnetic beads and ac4C antibody were rotated and incubated at room temperature for 1 h to bind the antibody to the magnetic beads. Then the RNA fragments and the antibody bound with magnetic beads were rotated at 4°C and incubated for 4 h to bind the RNA to the antibody. The combined complex is washed several times, and the RNA is further eluted from the complex. RNA sequencing libraries were constructed using the GenSeq® Low Input Whole RNA Library Prep Kit (GenSeq, Inc.). The constructed library was quality-controlled with Agilent 2100 bioanalyzer and then high-throughput sequenced on Illumina's NovaSeq sequencer. After Illumina NovaSeq 6000 sequencing, image analysis, base identification and quality control, Raw reads (Raw Data) were generated. First use Q30 for quality control. Then, cutadapt software (v1.9.3) was used to de-connect, remove low-quality reads, and obtain high-quality clean reads. The de-coupling reads were aligned to the reference genome using Hisat2 software (v2.0.4). MACS software was then used to identify the acetylation genes in each sample. diffReps software was used to identify differentially acetylated genes. The peaks located on the exon of mRNA were screened using a proprietary procedure and annotated accordingly. The genes encoding differential acetylation were analyzed by GO and Pathway.

2.22. RNA-seq

The high throughput RNA sequencing service is provided by CloudSeq Inc. (Shanghai, China). The procedure is described as follows: According to the supplier's instructions, ribosomal RNA (rRNA) will be removed using the GenSeq® rRNA Removal Kit (GenSeq, Inc.) kit. After the removal of rRNA, sequencing libraries were constructed using the GenSeq® Low Input RNA Library Prep Kit (GenSeq, Inc.) kit according to the vendor's instructions. The constructed sequencing library was quality-controlled and quantified by the BioAnalyzer 2100 system (Agilent Technologies, USA), and then double-ended 150bp sequencing was performed by Illumina NovaSeq 6000 instrument. The original data were sequenced by Illumina NovaSeq 6000 sequencer. Firstly, the Q30 value is used for raw data quality control. cutadapt software (v1.9.3) was used to remove connections, remove low-quality reads, and obtain high-quality clean reads. Clean reads were compared to the mouse reference genome (mm10) using hisat2 software, then raw count numbers were obtained using HTSeq software (v0.9.1), normalized using edgeR and multiple changes and p-value between the two groups of samples were calculated. Screening for differentially expressed genes. GO function and KEGG pathway were analyzed using differentially expressed mRNA.

2.23. Chromatin immunoprecipitation (ChIP)

ChIP analysis was performed using a chromatin immunoprecipitation kit (Thermo scientific, Germany) according to the manufacturer's protocol. Briefly, primary cardiomyocytes were inoculated with 5×10^7 cells in a culture dish with a diameter of 10 cm, overexpressed p53 plasmid was transfected, and empty plasmid was used as control. Cells were crosslinked with 1% formaldehyde at room temperature (10 min) after 48 h, quenched with cold 0.125 M 12 glycine for 5 min. Then the culture dish was washed with cold PBS twice for 5 min each time. Cardiomyocytes were collected using a pre-cooled cell lysis buffer, which was ultrasound-treated to produce chromatin fragments with an average length of about 500–800 bp. Overnight incubation was performed with anti-p53 antibody or anti-mouse IgG antibody in rotation at 4°C. 20 μL of evenly mixed ChIP-grade Protein A/G Plus agar-agar beads were added into the immune complex, incubated at 4°C for 1 h, eluted with IP washing solution 2–3 times, and purified DNA was collected for subsequent PCR detection.

2.24. Co-immunoprecipitation (Co-IP)

Tissues were lysed with IP lysis buffer (Beyotime, Shanghai, China), and protease inhibitor (Sigma-Aldrich Corporation, United Stats) was added. The cells were incubated on ice for 5 min, vortexed 30 s for 3 time and stood on ice. Then samples were centrifuged at 4°C 12000 r/min for 15 min and removed the supernatant. After the pre-clearing step with Protein G Magnetic Beads (MedChemExpress, United Stats), cell lysate (0.5 mg) was subjected to IP with the indicated antibodies (anti-P300 antibody, Abcam, ab275378, 1:50 dilution, IgG, Abcam, ab172730, 2 μg) overnight at 4 °C. Protein G-beads enriched antibodies were added to the mixture and rotated at 4 °C overnight. Then, immune complexes were washed three times in cold lysis buffer. The input and IP samples were resolved by SDS-PAGE and detected by immunoblot analysis with the indicated primary antibodies: anti-GAPDH antibody, anti-p53 antibody and anti-P300. **(Supplementary Table 4).**

2.25. Luciferase

Dual-Luciferase Reporter Assay System (Promega) was used to perform luciferase activity assay according to the manufacturer's instructions. Constructed NAT10-promoter-luc-Vector or NAT10-promoter-luc and transcription factor p53 plasmids were transfected into cells using Lipofectamine 2000 (Invitrogen). Meanwhile, renilla plasmid was transfected as internal reference. At 48 h after infection, luciferase activity was measured. The fluorescein activity was read by Tecan Infinite 200 (Tecan, männedorf , Switzerland).

2.26. Cell viability assay

Neonatal cardiomyocytes were seeded in 96-well plates at 8×10^4 cells per well. After each treatment according to the experimental requirements, the culture medium was changed into 100 μL DMEM and 10 μL CCK8 solution (Meilunbio, Dalian, China) per well, and then incubated at 37°C in the dark for 1.5–2 h. The result quantified with absorbance at 450 nm on a microplate reader (Bio Tek, Richmond, VA, USA).

2.27. RNA degradation assay

Cardiomyocytes seeded in 6-well plates were treated according to the experimental requirements. Actinomycin D (5 μg/ml) was added at 0 h, 4 h, and 8 h before total RNA extraction to extract RNA and detect the expression by PCR.

2.28. Statistical analysis

Each experiment was repeated at least three times. The data are expressed as the mean ± SEM calculated by GraphPad Prism 6.0 (GraphPad Software Inc., San Diego, CA) For multiple comparisons, one-way analysis of variance (ANOVA) followed by Tukey post hoc test was performed. The unpaired two-sided Student's t-test was used for the comparison between two groups. When $p < 0.05$, the results were considered statistically significant.

3. Results

3.1. p53 transcriptionally activates NAT10 during I/R

Although a recent study reported that NAT10 is involved in cardiomyocyte apoptosis in vitro [14], whether NAT10 is altered during cardiac I/R remains unknown. To this end, we established a mouse model of I/R in vivo and a cellular model of H/R stimulation-induced oxidative stress in vitro. Western blotting and qPCR revealed that the mRNA and protein levels of NAT10 were significantly elevated in both I/R-exposed hearts and H/R-exposed cardiomyocytes (Fig. 1A–B, Supplementary Figs. 1A–1B); these effects were accompanied by a marked increase in the ac4C levels of total RNA, as determined by a dot blotting assay (Supplementary Fig. 1C). Consistent with these findings, NAT10 protein levels were increased in adult mouse cardiomyocytes isolated from the infarct border zone of I/R-exposed hearts (Supplementary Figs. 1D–1E). It has been reported that the upregulation of NAT10 in response to DNA damage is abolished in p53-deficienet cells, suggesting that p53 may act as a regulator of NAT10 [26]. We next mapped the promoter region of NAT10 and found that NAT10 has a potential p53 binding motif according to the JASPAR database. These findings prompted us to investigate whether p53 is an upstream activator of NAT10 in mouse hearts post-I/R. To test this hypothesis, luciferase reporter plasmids containing the NAT10 promoter sequence and an empty plasmid serving as a negative control were constructed and transfected into HEK293 cells. A luciferase reporter assay showed that p53 activated the NAT10 promoter, as demonstrated by increased luciferase activity (Fig. 1C). Furthermore, chromatin immunoprecipitation (ChIP) assays revealed that the NAT10 promoter region was obviously enriched in the p53-precipitated cardiomyocyte fraction after p53 was overexpressed (Fig. 1D), suggesting that p53 directly bound to the NAT10 promoter region. To confirm this result, we examined NAT10 expression in cardiomyocytes after overexpressing or silencing p53. The results showed that p53 siRNA treatment reduced p53 expression in both normoxia-exposed and H/R-exposed cardiomyocytes, and this

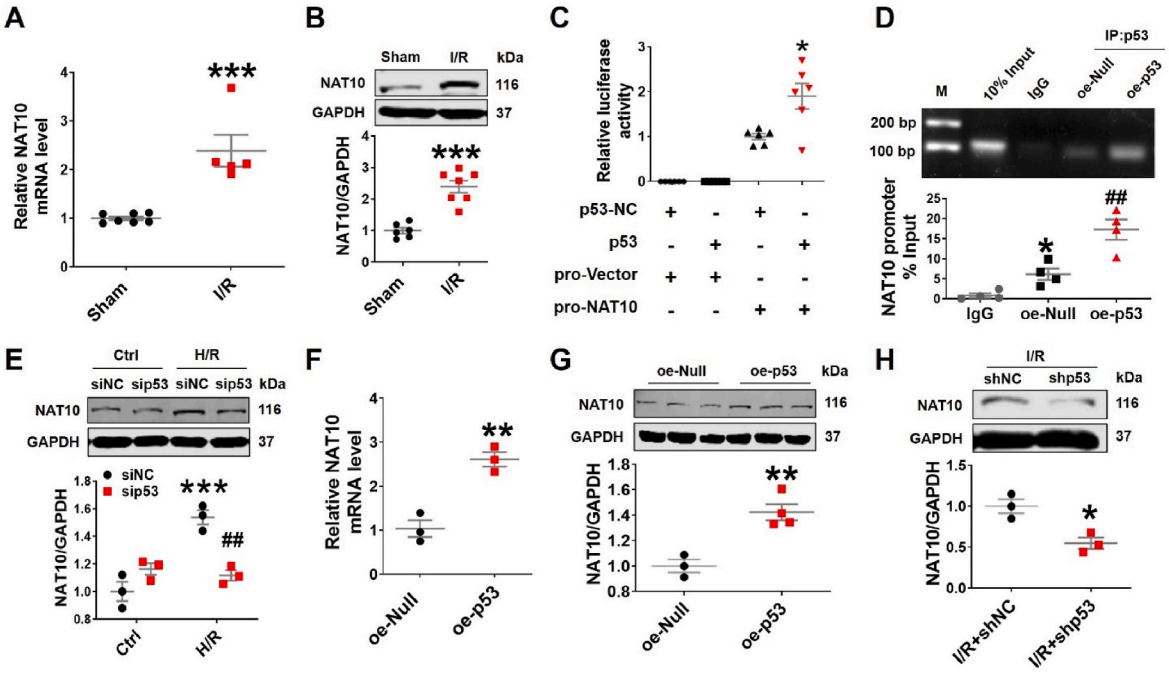

Fig. 1. p53 transcriptional activates NAT10 during I/R surgery.
(A) The NAT10 mRNA level in ischemia–reperfusion (45 min for ischemia and 24 h for reperfusion, I/R) and Sham-operated hearts were analyzed by qRT-PCR. Sham n = 7, I/R n = 5. ***p < 0.001 vs Sham. **(B)** The protein level of NAT10 in I/R and Sham-operated hearts were analyzed by Western blotting. Sham n = 6, I/R n = 7. ***p < 0.001 vs Sham. **(C)** Detection of p53 plasmid activating NAT10 promoter(pro-NAT10) in HEK293 cells by luciferase report. n = 6. *p < 0.05 vs pro-NAT10-NC. **(D)** ChIP analysis of p53 binding to the promoter of NAT10. Cardiomyocytes were treated with p53 and null plasmid at indicated time. ChIP was performed with p53 or IgG antibody. oe-Null n = 4. *p < 0.05 vs IgG. oe-p53 n = 4. ##p < 0.01 vs oe-Null. **(E)** Cardiomyocytes were infected with siRNA. The protein level of NAT10 in infection cardiomyocytes with H/R was analyzed by Western blotting. Ctrl + siNC n = 3, Ctrl + sip53 n = 3, H/R + siNC n = 3, H/R + sip53 n = 3. ***p < 0.001 vs Ctrl + siNC, ##p < 0.01 vs H/R + siNC. **(F)** The NAT10 mRNA level in cardiomyocytes with p53 plasmid was analyzed by qRT-PCR. n = 3. **p < 0.01 vs oe-Null. **(G)** Cardiomyocytes were infected with p53 plasmid. The protein level of NAT10 in infection cardiomyocytes were analyzed by Western blotting. oe-Null n = 3, oe-p53 n = 4. **p < 0.01 vs oe-Null. **(H)** The NAT10 protein detected by Western blot. I/R + AAV9-shNC n = 3, I/R + AAV9-shp53 n = 3. *p < 0.05 vs I/R + AAV9-shNC. Data are represented as mean ± SEM.

downregulation led to a marked decrease in the mRNA and protein levels of NAT10 after H/R (Fig. 1E, Supplementary Figs. 1F–1I). In contrast, compared with those in p53-NC-transfected cardiomyocytes, the overexpression of p53 in cardiomyocytes by transfection with the p53 overexpression plasmid markedly elevated the mRNA and protein levels of NAT10 (Fig. 1F–G, Supplementary Figs. 1J–1K). Then, p53 was knocked down in vivo via the administration of adeno-associated virus 9 (AAV9) carrying p53 shRNA (AAV9-shp53) by tail vein injection. Consistent with the in vitro results, knockdown of p53 in vivo significantly decreased the I/R-induced upregulation of NAT10 at the mRNA and protein levels (Fig. 1H, Supplementary Fig. 1L-1N). Taken together, these results demonstrate that p53 can induce NAT10 transcription during I/R injury.

3.2. *NAT10 exacerbated H/R-induced ferroptosis in cardiomyocytes*

To examine the function of NAT10 in cardiomyocyte ferroptosis, we performed gain-of-function and loss-of-function experiments in vitro. Neonatal mouse cardiomyocytes were isolated and subjected to hypoxia-reoxygenation (H/R). Transfection of the cardiomyocytes with an adenovirus harboring the NAT10 gene led to increased NAT10 mRNA and protein levels in the presence or absence of H/R exposure (Supplementary Figs. 2A–2B). Overexpression of NAT10 reduced cell viability in the presence or absence of H/R exposure (Fig. 2A). NAT10 overexpression caused a marked increase in lipid-ROS level and a decrease in GPX4 protein level (Fig. 2B–D). In contrast, siRNA-mediated knockdown of NAT10 markedly abrogated the H/R-induced upregulation of NAT10 expression (Supplementary Fig. 2C), and this downregulation led to increased cell viability (Fig. 2E). In addition, knockdown of NAT10 attenuated the increase in lipid-ROS levels and decrease in GPX4 protein levels that were induced by H/R in cardiomyocytes (Fig. 2F–H). These results suggest that NAT10 contributes to cardiomyocyte ferroptosis.

3.3. *Deficiency of NAT10 protects against I/R-induced cardiac ferroptosis*

To study the potential role of NAT10 in cardiac ferroptosis during I/R injury, we established cardiomyocyte-specific NAT10-knockout mice ($NAT10^{f/+/Myh6-Cre}$, designated $NAT10^{CKO}$ hereafter) by crossing $NAT10^{f/+}$ (designated $NAT10^{f/+}$ hereafter) mice with Myh6-Cre mice. Western blotting results confirmed the marked downregulation of NAT10 protein expression in the heart tissues and isolated adult cardiomyocytes from $NAT10^{CKO}$ mice compared to those in $NAT10^{f/+}$ littermate controls (**Supplementary Figs. 3A–3B**). However, the NAT10 protein expression in non-cardiomyocytes was unchanged (Supplementary Fig. 3B). $NAT10^{CKO}$ and $NAT10^{f/+}$ mice were subsequently subjected to cardiac I/R surgery. I/R induced cardiac injury, as indicated by the increases in the plasma levels of lactate dehydrogenase (LDH) and creatine kinase isoenzyme-MB (CKMB) in $NAT10^{f/+}$ mice after I/R; however, these effects were significantly attenuated in $NAT10^{CKO}$ mice (Fig. 3A–B). The results of Evans blue and triphenyltetrazolium chloride staining showed that post-I/R infarct size was reduced in $NAT10^{CKO}$ mice compared to $NAT10^{f/+}$ mice (Fig. 3C). Moreover, echocardiographic analysis of $NAT10^{f/+}$ mice revealed pronounced decreases in the I/R-induced cardiac ejection fraction (EF%) and fractional shortening (FS%), and these changes were largely reversed in $NAT10^{CKO}$ mice (Fig. 3D). In addition, the I/R-induced decrease in the ferroptosis-related marker GPX4 was strikingly higher

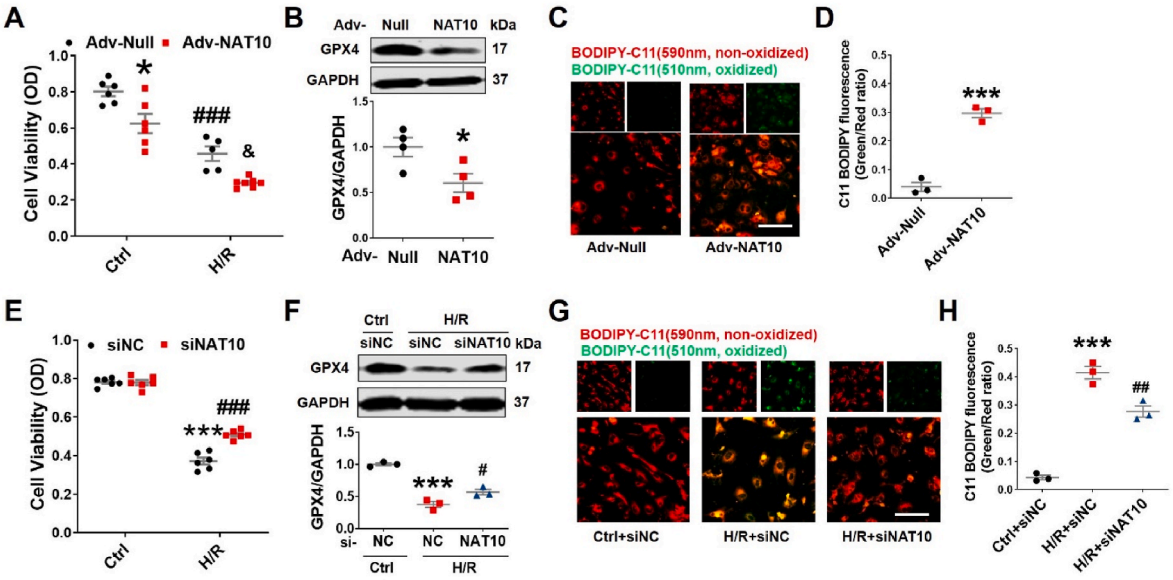

Fig. 2. NAT10 aggravates H/R-induced cardiomyocytes damage
(A) Cell viability was detected with CCK8 assay kit. Ctrl + Adv-Null n = 6, Ctrl + Adv-NAT10 n = 6, H/R + Adv-Null n = 5, H/R + Adv-NAT10 n = 7. *p < 0.05 vs Ctrl + Adv-Null, ###p < 0.001 vs Ctrl + Adv-Null, &p < 0.05 vs H/R + Adv-Null. **(B)** GPX4 protein level. Adv-Null n = 4, Adv-NAT10 n = 4. *p < 0.05 vs Adv-Null. **(C–D)** Analysis of lipid-ROS using C11 BODIPY 581/591 fluorescence staining (Bar:20 μm), Red, non-oxidized form of C11 BODIPY; Green, oxidized form of C11 BODIPY. Adv-Null n = 3, Adv-NAT10 n = 3 (3 fields per sample). ***p < 0.001 vs Adv-Null. **(E)** Cell viability was detected with CCK8 assay kit. Ctrl + siNC n = 6, Ctrl + siNAT10 n = 6, H/R + siNC n = 6, H/R + siNAT10 n = 6. ***p < 0.001 vs Ctrl + siNC, ###p < 0.001 vs H/R + siNC. **(F)** GPX4 protein level. Ctrl + siNC n = 3, H/R + siNC n = 3, H/R + siNAT10 n = 3. ***p < 0.001 vs Ctrl + siNC, #p < 0.05 vs H/R + siNC. **(G–H)** Analysis of lipid-ROS using C11 BODIPY 581/591 fluorescence staining (Bar:20 μm), Red, non-oxidized form of C11 BODIPY; Green, oxidized form of C11 BODIPY. Ctrl + siNC n = 3, H/R + siNC n = 3, H/R + siNAT10 n = 3 (3 fields per sample). ***p < 0.001 vs Ctrl + siNC, ##p < 0.01 vs H/R + siNC. Data are represented as mean ± SEM. (For interpretation of the references to colour in this figure legend, the reader is referred to the Web version of this article.)

in NAT10^{CKO} mice than in NAT10$^{f/+}$ mice (Fig. 3E). Similar to the findings of previous studies [7,23,24], transmission electron microscopy revealed morphological features of ferroptosis in cardiomyocytes from I/R mice, as indicated by the presence of distorted mitochondria, increased mitochondrial membrane density and reduced mitochondrial size. However, these effects were alleviated by NAT10 knockdown (Fig. 3F–G). Moreover, NAT10 deficiency significantly reduced the levels of the lipid peroxidation (Fig. 3F, bottom; Fig. 3H) in I/R-exposed hearts. To further confirm the therapeutic potential of manipulating NAT10 expression, we generated an AAV9-shNAT10 construct to knock down NAT10 in mouse hearts. As expected, knockdown of NAT10 markedly ameliorated cardiac function and inhibited cardiomyocyte ferroptosis in I/R-exposed hearts compared with those in AAV9-shNC-treated mice **(Supplementary Figs. 3C–3H)**. These results demonstrate that NAT10 deficiency attenuates cardiac I/R injury by inhibiting cardiac ferroptosis.

3.4. *NAT10 induces cardiac ferroptosis to exacerbate cardiac I/R injury*

To further investigate the role of NAT10 in cardiomyocyte ferroptosis in vivo, we induced cardiomyocyte-specific overexpression of NAT10 via the delivery of an AAV9 vector encoding NAT10 (AAV9-NAT10) by tail vein injection. Successful NAT10 overexpression in both sham and I/R-exposed mouse hearts were verified by Western blotting (Supplementary Fig. 4A). In contrast to the findings in NAT10^{CKO} mice, overexpression of NAT10 alone was sufficient to increase the plasma levels of LDH and CKMB in the absence of I/R, and NAT10 overexpression promoted the release of these enzymes post-I/R (Fig. 4A–B). The I/R-induced increase in cardiac infarct size was further augmented by NAT10 overexpression (Fig. 4C). The I/R-induced detrimental effects, as indicated by cardiac functional impairments, were further exacerbated by NAT10 overexpression (Fig. 4D–E). Transmission electron microscopy analysis revealed that overexpression of NAT10 was sufficient to cause mitochondrial disruption at baseline, as indicated by increased mitochondrial membrane density and decreased mitochondrial size (Fig. 4F–G). NAT10 overexpression exacerbated the mitochondrial impairment that was observed after I/R (Fig. 4F–G). Moreover, overexpression of NAT10 elevated the GPX4 protein levels and lipid peroxidation levels in mouse hearts (Fig. 4H–I). To further confirm the dominant role of NAT10 in triggering cardiac ferroptosis upon I/R, we treated mice with Fer-1 (an inhibitor of ferroptosis) or emricasan (an inhibitor of apoptosis) by intraperitoneal injection prior to I/R induction. As expected, treatment with Fer-1 or emricasan significantly inhibited the CKMB and LDH release, reduced the myocardial infarct size, and alleviated the cardiac dysfunction that were induced by NAT10 in I/R-exposed hearts (Fig. 4J–M). More importantly, treatment with Fer-1 exerted far superior cardioprotective effects than treatment with emricasan according to the abovementioned parameters. Consistent with in vivo results, Fer-1 treatment attenuated cardiomyocytes ferroptosis and rescued the loss of cell viability in cultured cardiomyocytes induced by NAT10 overexpression **(Supplementary Figs. 4B–4E)**. These results suggest that ferroptosis induced by NAT10 plays a much more important role during I/R injury.

3.5. *NAT10 enhances the stabilization of Mybbp1a via ac4C modification*

To explore the molecular mechanism by which NAT10 exacerbates cardiomyocyte ferroptosis during I/R, we performed an ac4C acetylated RNA immunoprecipitation sequencing (acRIP-seq) assay to map the transcriptomic ac4C profile of RNA isolated from 3 pairs of Sham and I/R-exposed hearts. A total of 14805 ac4C peaks enriched in 5665 genes were identified in Sham-operated hearts, while 14921 ac4C peaks enriched in 6243 genes were identified in I/R-exposed hearts. I/R-exposed and Sham mouse hearts shared 11289 common ac4C peaks enriched in 4770 genes, which accounted for 75.66% of the total acetylated peaks in I/R-exposed hearts and 76.25% in Sham hearts

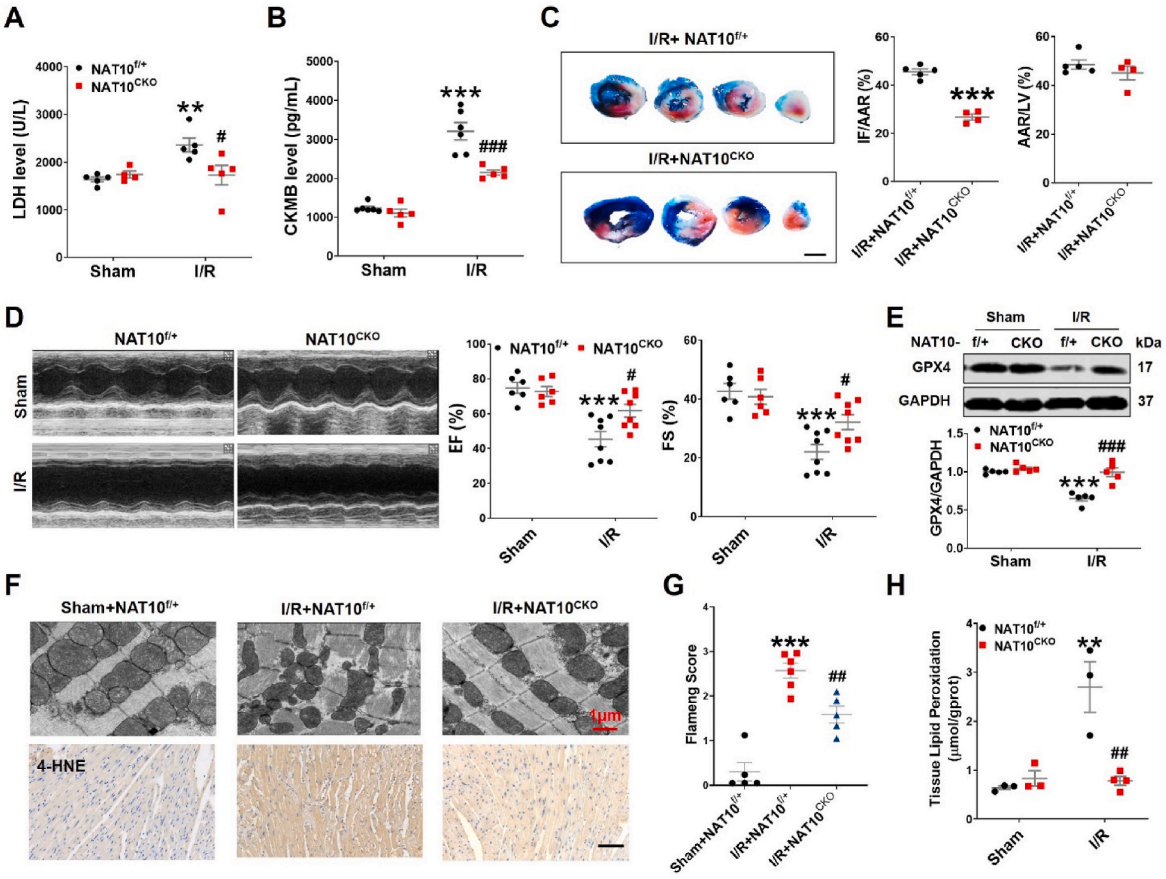

Fig. 3. Deficiency of NAT10 protects against I/R-induced cardiac injury.
(A) Plasma LDH was analyzed by a LDH assay kit. Sham + $NAT10^{f/+}$ n = 5, Sham + $NAT10^{CKO}$ n = 4, I/R + $NAT10^{f/+}$ n = 5, I/R + $NAT10^{CKO}$ n = 5. **p < 0.01 vs Sham + $NAT10^{f/+}$, #p < 0.05 vs I/R + $NAT10^{f/+}$. **(B)** Plasma CKMB level was analyzed by Elisa assay. Sham + $NAT10^{f/+}$ n = 6, Sham + $NAT10^{CKO}$ n = 5, I/R + $NAT10^{f/+}$ n = 6, I/R + $NAT10^{CKO}$ n = 4. ***p < 0.001 vs Sham + $NAT10^{f/+}$, ###p < 0.001 vs I/R + $NAT10^{f/+}$. **(C)** Infarct size of I/R hearts by Evans blue/TTC double staining (scale bar: 2 mm). IF: Infarct Area; AAR: Area at risk; LV: Left ventricle. I/R + $NAT10^{f/+}$ n = 5, I/R + $NAT10^{CKO}$ n = 4. ***p < 0.001 vs I/R + $NAT10^{f/+}$. **(D)** Representative images of echocardiographs and statistics of ejection fraction (EF), fractional shortening (FS). Sham + $NAT10^{f/+}$ n = 6, Sham + $NAT10^{CKO}$ n = 6, I/R + $NAT10^{f/+}$ n = 8, I/R + $NAT10^{CKO}$ n = 8. ***p < 0.001 vs Sham + $NAT10^{f/+}$, #p < 0.05 vs I/R + $NAT10^{f/+}$. **(E)** GPX4 protein level. Sham + $NAT10^{f/+}$ n = 5, Sham + $NAT10^{CKO}$ n = 5, I/R + $NAT10^{f/+}$ n = 5, I/R + $NAT10^{CKO}$ n = 5. ***p < 0.001 vs Sham + $NAT10^{f/+}$, ###p < 0.001 vs I/R + $NAT10^{f/+}$. **(F)** Transmission electron microscope representation of mouse heart tissue (**top**, Bar: 1 μm) and Immunohistochemical staining of 4-HNE in the heart tissues of mice 24 h after ischemia reperfusion injury (**bottom**, n = 3 per group, 4–5 fields per sample. Bar:50 μm). **(G)** Flameng scores assessed the degree of mitochondrial damage in mice heart tissue. Sham + $NAT10^{f/+}$ n = 5, I/R + $NAT10^{f/+}$ n = 6, I/R + $NAT10^{CKO}$ n = 5. ***p < 0.001 vs Sham + $NAT10^{f/+}$, ##p < 0.01 vs I/R + $NAT10^{f/+}$. **(H)** Tissue Lipid peroxidation level was analyzed by Lipid-peroxidation assay kit. Sham + $NAT10^{f/+}$ n = 3, Sham + $NAT10^{CKO}$ n = 3, I/R + $NAT10^{f/+}$ n = 3, I/R + $NAT10^{CKO}$ n = 4. **p < 0.01 vs Sham + $NAT10^{f/+}$, ##p < 0.01 vs I/R + $NAT10^{f/+}$. Data are represented as mean ± SEM. (For interpretation of the references to colour in this figure legend, the reader is referred to the Web version of this article.)

(Supplementary Fig. 5A). The ac4C peaks in the sham and I/R-exposed hearts were mainly distributed in coding regions and 3′-UTRs as well as in start and stop codons (Supplementary Fig. 5B). Consistent with the findings of a previous study [25], the ac4C motif "A(U)GCA(U)GC" was most commonly enriched in the ac4C peaks (Supplementary Fig. 5C). In addition, after analyzing the RNA-seq data, we correlated the levels of the ac4C peaks with gene expression. Consistent with the finding that ac4C modification enhances mRNA stability [13], our results showed that 2342 ac4C peaks from 1481 hyper-upregulated genes were increased (termed hyperacetylated ac4C peaks), while 1326 ac4C peaks from 1109 hyper-downregulated genes were decreased (termed hypo-acetylated ac4C peaks) in I/R-exposed hearts relative to sham-operated control hearts (FC > 2, P < 0.00001) (Fig. 5A). Gene Ontology (GO) enrichment analysis of genes associated with biological processes and molecular functions revealed that genes with hyperacetylated ac4C in I/R-exposed hearts were related mainly to the regulation of biological processes, cellular processes, and protein binding (Supplementary Fig. 5D). To screen the potential targets of NAT10, we first performed qPCR assays on the differentially methylated genes that were implicated in cell death in mouse hearts. Among these 12 genes, Mybbp1a, Ddx21 and Pabpc1 were significantly upregulated in I/R-exposed hearts but downregulated after NAT10 was knocked down (Fig. 5B–C). To further verify the acRIP-seq results, we performed an acRIP-qPCR assay on the ac4C-acetylated genes in cardiomyocytes (Fig. 5D, Supplementary Figs. 5E–5F). As shown in Fig. 5D, Mybpp1a was significantly enriched in the anti-NAT10-immunoprecipitated fraction relative to the anti-IgG fraction, and this enrichment was further enhanced by NAT10 over-expression (Fig. 5D). Visualization of the acRIP-seq and mRNA-seq results also revealed a greater abundance of ac4C modification peaks in the CD region and 3′-UTR of Mybbp1a mRNA in I/R-exposed hearts than in Sham-operated hearts, and this finding was accompanied by a marked increase in Mybbp1a mRNA expression (Supplementary Fig. 5G). Since NAT10 increases the mRNA and protein levels of Mybb1pa, we carried out an RNA decay experiment in cardiomyocytes by treating them with actinomycin D. The results showed that the actinomycin D-induced degradation of Mybb1pa mRNA was prevented by the overexpression of NAT10 (Fig. 5E–F). Furthermore, we found that the Mybpp1a protein level was markedly elevated in I/R-exposed hearts and that this change

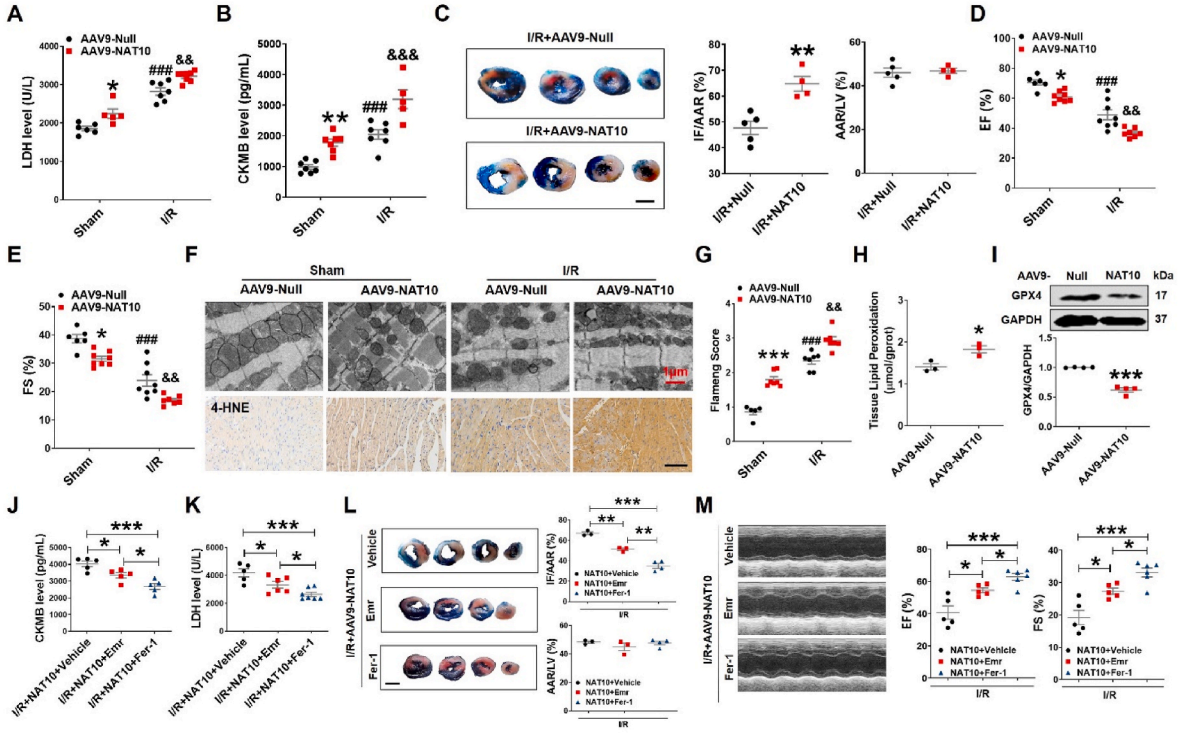

Fig. 4. NAT10 exacerbates cardiac I/R injury

(A) Plasma LDH was analyzed by a LDH assay kit. Sham + AAV9-Null n = 6, Sham + AAV9-NAT10 n = 5, I/R + AAV9-Null n = 7, I/R + AAV9-NAT10 n = 8. *p < 0.05 vs Sham + AAV9-Null, $^{\#\#\#}$p < 0.001 vs Sham + AAV9-Null, $^{\&\&}$p < 0.01 vs I/R + AAV9-Null. **(B)** Plasma CKMB level was analyzed by Elisa assay. Sham + AAV9-Null n = 7, Sham + AAV9-NAT10 n = 7, I/R + AAV9-Null n = 7, I/R + AAV9-NAT10 n = 7. **p < 0.01 vs Sham + AAV9-Null, $^{\#\#\#}$p < 0.001 vs Sham + AAV9-Null, $^{\&\&\&}$P < 0.001 vs I/R + AAV9-Null. **(C)** Infarct size of I/R hearts by Evans blue/TTC double staining (scale bar: 2 mm). IF: Infarct Area; AAR: Area at risk; LV: Left ventricle. I/R + AAV9-Null n = 5, I/R + AAV9-NAT10 n = 4. **p < 0.01 vs I/R + AAV9-Null. **(D–E)** Representative images of echocardiographs and statistics of ejection fraction (EF), fractional shortening (FS). Sham + AAV9-Null n = 6, Sham + AAV9-NAT10 n = 8, I/R + AAV9-Null n = 8, I/R + AAV9-NAT10 n = 7. *p < 0.05 vs Sham + AAV9-Null, $^{\#\#\#}$p < 0.001 vs Sham + AAV9-Null, $^{\&\&}$p < 0.01 vs I/R + AAV9-Null. **(F)** Transmission electron microscope representation of mouse heart tissue (**top**, Bar: 1 μm) and Immunohistochemical staining of 4-HNE in the heart tissues of mice 24 h after ischemia reperfusion injury (**bottom**, n = 3 per group, 4–5 fields per sample. Bar:50 μm). **(G)** Flameng scores assessed the degree of mitochondrial damage in mice heart tissue. Sham + AAV9-Null n = 5, Sham + AAV9-NAT10 n = 7. I/R + AAV9-Null n = 7, I/R + AAV9-NAT10 n = 7. ***p < 0.001 vs Sham + AAV9-Null. $^{\#\#\#}$p < 0.001 vs Sham + AAV9-Null, $^{\&\&}$p < 0.01 vs I/R + AAV9-Null. **(H)** Tissue Lipid peroxidation level was analyzed by Lipid-peroxidation assay kit. AAV9-Null n = 3, AAV9-NAT10 n = 3. *p < 0.05 vs AAV9-Null. **(I)** GPX4 protein level. AAV9-Null n = 4, AAV9-NAT10 n = 4. ***p < 0.001 vs AAV9-Null. **(J)** Plasma CKMB level was analyzed by creatine kinase isoenzyme MB assay kit. I/R + AAV9-NAT10+Vehicle n = 5, I/R + AAV9-NAT10+Fer-1 n = 5, I/R + AAV9-NAT10 + Emr n = 5, ***p < 0.001 vs I/R + AAV9-NAT10+Vehicle, *p < 0.05 vs I/R + AAV9-NAT10+Vehicle. **(K)** Plasma LDH activity was analyzed by lactate dehydrogenase assay kit. I/R + AAV9-NAT10+Vehicle n = 5, I/R + AAV9-NAT10+Fer-1 n = 6, I/R + AAV9-NAT10 + Emr n = 7, ***p < 0.001 vs I/R + AAV9-NAT10+Vehicle, *p < 0.05 vs I/R + AAV9-NAT10+Vehicle. **(L)** Infarct size of I/R hearts by TTC staining (scale bar: 2 mm). I/R + AAV9-NAT10+Vehicle n = 6, I/R + AAV9-NAT10+Fer-1 n = 5, I/R + AAV9-NAT10 + Emr n = 5, ***p < 0.001 vs I/R + AAV9-NAT10+Vehicle, **p < 0.01 vs I/R + AAV9-NAT10+Vehicle. **p < 0.01 vs I/R + AAV9-NAT10 + Emr. **(M)** Representative images of echocardiographs and statistics of ejection fraction (EF), fractional shortening (FS). I/R + AAV9-NAT10+Vehicle n = 5, I/R + AAV9-NAT10+Fer-1 n = 5, I/R + AAV9-NAT10 + Emr n = 6, ***p < 0.001 vs I/R + AAV9-NAT10+Vehicle *p < 0.05 vs I/R + AAV9-NAT10+Vehicle. Data are represented as mean ± SEM. (For interpretation of the references to colour in this figure legend, the reader is referred to the Web version of this article.)

was abrogated by NAT10 deficiency (Fig. 5G). In contrast, overexpression of NAT10 increased Mybbp1a protein expression in the presence or absence of I/R treatment (Fig. 5H). Consistent with these findings, knockdown of NAT10 reversed the H/R-induced increase in Mybbp1a protein expression in cardiomyocytes in vitro (Supplementary Fig. 5H). Furthermore, overexpression of NAT10 increased the Mybbp1a protein level in the presence or absence of H/R treatment (Supplementary Fig. 5I). These results suggest that Mybbp1a may act as a downstream target of NAT10 during cardiac I/R injury.

It has been shown that MYB binding protein 1A (Mybbp1a) activates p53 by promoting its acetylation, thereby inducing cell death in response to cellular stress [26]. These findings prompted us to investigate whether Mybbp1a is involved in H/R stimulation-induced ferroptosis. To this end, we transfected Mybbp1a siRNAs into cardiomyocytes to knock down Mybbp1a expression. Western blotting analysis showed that siRNA#2 exerted the strongest effect on silencing Mybbp1a compared to the other constructs (Supplementary Fig. 6A); therefore, this sequence was used for the following study. To further confirm whether Mybbp1a knockdown can mitigate I/R-induced cardiac injury in vivo, we generated a AAV9-shMybbp1a construct to silence Mybbp1a expression in mouse hearts. As shown in Supplementary Fig. 6B, the administration of AAV9-shMybbp1a resulted in a significant reduction in Mybbp1a protein levels in both Sham and I/R-exposed hearts. Compared with AAV9-shNC, Mybbp1a knockdown markedly reduced the infarct size and plasma LDH and CKMB levels of I/R-exposed (Fig. 5I–K). In addition, knockdown of Mybbp1a markedly ameliorated I/R-induced cardiac dysfunction (Fig. 5L). Notably, I/R-induced cardiac ferroptosis was attenuated by Mybbp1a knockdown, as indicated by increased GPX4 levels and decreased lipid peroxidation levels (Fig. 5M–O). Consistent with the in vivo results, we demonstrated that knockdown of Mybbp1a alleviated H/R-induced cardiomyocyte ferroptosis, as indicated by marked increases in GPX4 protein expression and the strong decrease in lipid-ROS production (Supplementary Figs. 6C–6D). These results suggest that the inhibition of Mybbp1a protects against I/R-induced cardiac injury by attenuating cardiomyocyte ferroptosis.

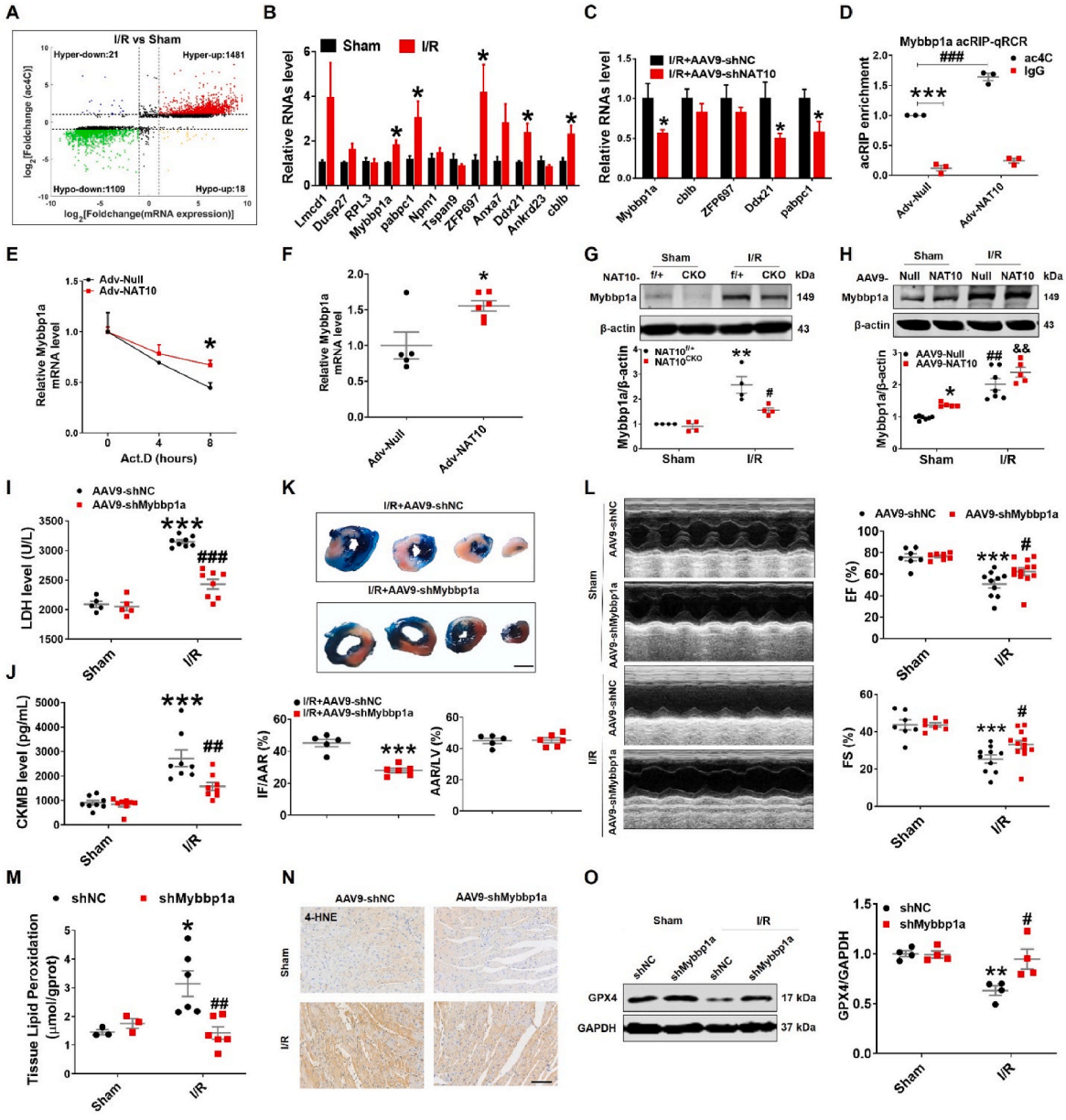

Fig. 5. NAT10 stabilizes Mybbp1a by inducing its ac4C modification.

(A) Correlation of changes in mRNAs levels and ac4C levels in the hearts of mice treated with I/R compared with Sham. (B) The level of ac4C target mRNAs in I/R. Sham n = 4–5, I/R n = 5–6. *p < 0.05 vs Sham. (C) The level of ac4C target mRNAs in AAV9-shNAT10 treated hearts after I/R. I/R + shNC n = 6–7, I/R + shNAT10 n = 6. *p < 0.05 vs I/R + shNC. (D) The ac4C modification level of Mybbp1a mRNA was detected by acRIP-qPCR. n = 3 ***p < 0.001 vs IgG, ###p < 0.001 vs Adv-Null. (E) Degradation of Mybbp1a mRNA in actinomycin-D (Act.D 5 μg/mL) treated cardiomyocytes. Adv-Null-0h n = 5, Adv-Null-4h n = 3, Adv-Null-8h n = 3, Adv-NAT10-0 h n = 6, Adv-NAT10-4 h n = 3, Adv-NAT10-8 h n = 3. *p < 0.05 vs Adv-NAT10-8 h. (F) Mybbp1a mRNA level in cardiomyocytes treated with Adv-NAT10. Adv-Null n = 5, Adv-NAT10 n = 6. *p < 0.05 vs Adv-Null. (G–H) Mybbp1a protein level in I/R hearts. (G) Sham + NAT10$^{f/+}$ n = 4 Sham + NAT10^{CKO} n = 4, I/R + NAT10$^{f/+}$ n = 4, I/R + NAT10^{CKO} n = 4 **p < 0.01 vs Sham + NAT10$^{f/+}$, #p < 0.05 vs I/R + NAT10$^{f/+}$. (H) Sham + AAV9-Null n = 7, Sham + AAV9-NAT10 n = 7, I/R + AAV9-Null n = 6, I/R + AAV9-NAT10 n = 6. *p < 0.05 vs Sham + AAV9-Null, ##p < 0.01 vs Sham + AAV9-Null, &&p < 0.01 vs I/R + AAV9-Null. (I) Plasma LDH was analyzed by a LDH assay kit. Sham + AAV9-shNC n = 5, Sham + AAV9-shMybbp1a n = 5, I/R + AAV9-shNC n = 8, I/R + AAV9-shMybbp1a n = 8. ***p < 0.001 vs Sham + AAV9-shNC, ###p < 0.001 vs I/R + AAV9-shNC. (J) Plasma CKMB level was analyzed by Elisa assay. Sham + AAV9-shNC n = 8, Sham + AAV9-shMybbp1a n = 8, I/R + AAV9-shNC n = 8, I/R + AAV9-shMybbp1a n = 8. ***p < 0.001 vs Sham + AAV9-shNC, ##p < 0.01 vs I/R + AAV9-shNC. (K) Infarct size of I/R hearts by Evans blue/TTC double staining (scale bar: 2 mm). IF: Infarct Area; AAR: Area at risk; LV: Left ventricle. I/R + AAV9-shNC n = 5, I/R + AAV9-shMybbp1a n = 6. ***p < 0.001 vs I/R + AAV9-shNC. (L) Representative images of echocardiographs and statistics of ejection fraction (EF), fractional shortening (FS). Sham + AAV9-shNC n = 7, Sham + AAV9-shMybbp1a n = 7, I/R + AAV9-shNC n = 10, I/R + AAV9-shMybbp1a n = 12. ***p < 0.001 vs Sham + AAV9-shNC, #p < 0.05 vs I/R + AAV9-shNC. (M) Tissue Lipid peroxidation level was analyzed by Lipid-peroxidation assay kit. Sham + AAV9-shNC n = 3, Sham + AAV9-shMybbp1a n = 3, I/R + AAV9-shNC n = 6, I/R + AAV9-shMybbp1a n = 6. *p < 0.05 vs Sham + AAV9-shNC, ##p < 0.01 vs I/R + AAV9-shNC. (N) Immunohistochemical staining of 4-HNE in the heart tissues of mice 24 h after myocardial reperfusion injury (n = 3 per group, 4–5 fields per sample. Bar:50 μm). (O) GPX4 protein level. Sham + AAV9-shNC n = 4, Sham + AAV9-shMybbp1a n = 4, I/R + AAV9-shNC n = 4, I/R + AAV9-shMybbp1a n = 4. **p < 0.01 vs Sham + AAV9-shNC, #p < 0.05 vs I/R + AAV9-shNC. Data are represented as mean ± SEM. (For interpretation of the references to colour in this figure legend, the reader is referred to the Web version of this article.)

3.6. NAT10 exacerbates cardiac I/R injury by regulating the Mybbp1a/p53 axis

Given the protective effects of Mybbp1a knockdown on cardiac I/R injury and the NAT10-mediated stabilization of Mybbp1a, we hypothesized that Mybbp1a may mediate the detrimental role of NAT10 in cardiac ferroptosis and I/R injury. To test this hypothesis, we knocked down Mybbp1a via tail vein injection of AAV9-shMybbp1a into NAT10-overxpressing mouse hearts. As expected, knockdown of Mybbp1a reduced the release of LDH and CKMB in I/R-exposed NAT10-

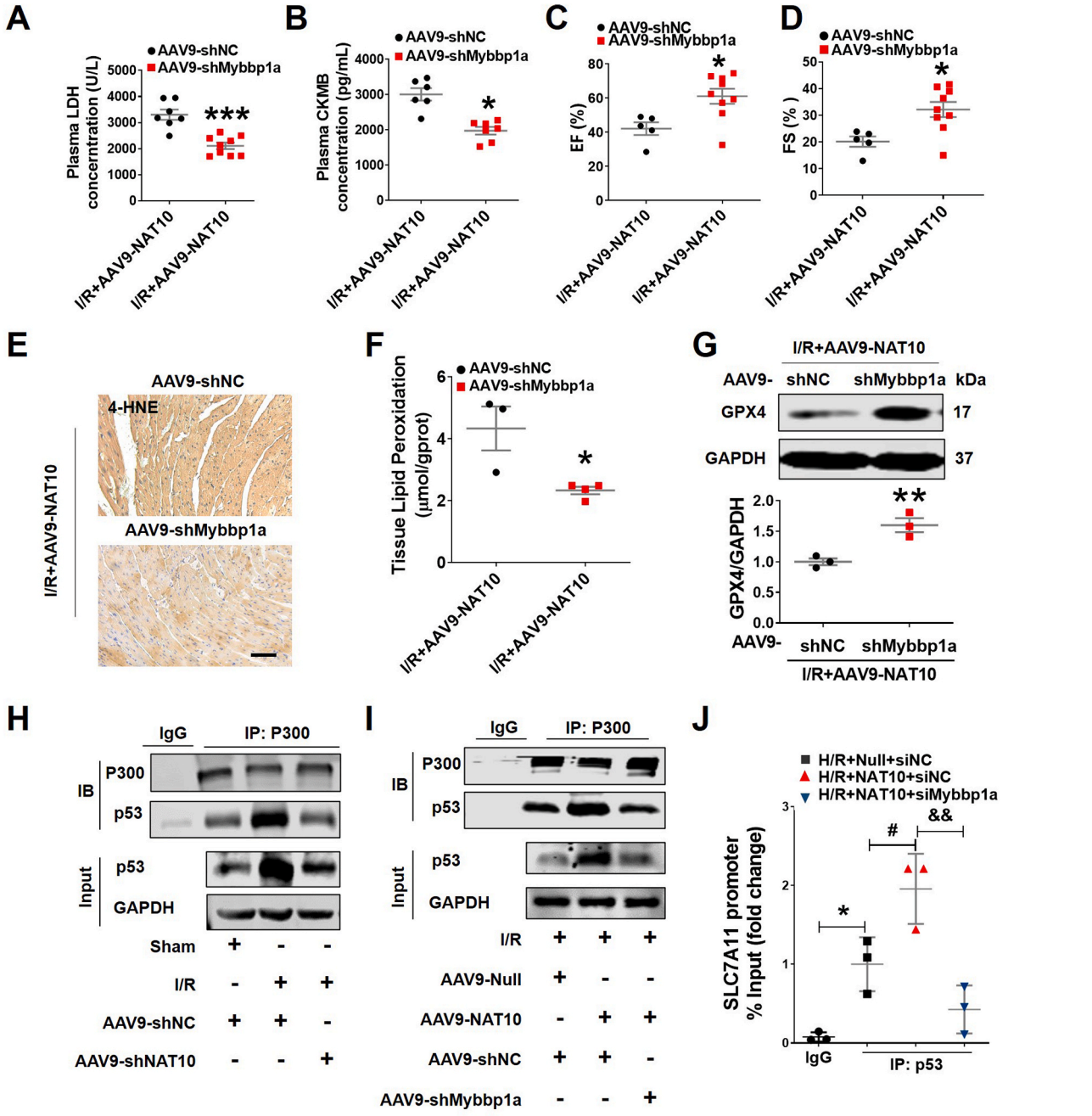

Fig. 6. Mybbp1a mediates NAT10 induced exacerbation on cardiac I/R injury.
(A) Plasma LDH was analyzed by a LDH assay kit. I/R + AAV9-NAT10 + AAV9-shNC n = 7, I/R + AAV9-NAT10 + AAV9-shMybbp1a n = 9. ***p < 0.001 vs I/R + AAV9-NAT10 + AAV9-shNC. (B) Plasma CKMB level was analyzed byElisa assay. I/R + AAV9-NAT10 + AAV9-shNC n = 7, I/R + AAV9-NAT10 + AAV9-shMybbp1a n = 7. *p < 0.05 vs I/R + AAV9-NAT10 + AAV9-shNC. (C–D) Representative images of echocardiographs and statistics of ejection fraction (EF) and fractional shortening (FS). I/R + AAV9-NAT10 + AAV9-shNC n = 5, I/R + AAV9-NAT10 + AAV9-shMybbp1a n = 9. *p < 0.05 vs I/R + AAV9-NAT10 + AAV9-shNC. (E) Immunohistochemical staining of 4-HNE in the heart tissues of mice 24 h after myocardial reperfusion injury (n = 3 per group, 4–5 fields per sample. Bar:50 μm). (F) Tissue Lipid peroxidation level was analyzed by Lipid-peroxidation assay kit. I/R + AAV9-NAT10 + AAV9-shNC n = 3, I/R + AAV9-NAT10 + AAV9-shMybbp1a n = 4. *p < 0.05 vs I/R + AAV9-NAT10 + AAV9-shNC. (G) GPX4 protein level. I/R + AAV9-NAT10 + AAV9-shNC n = 3, I/R + AAV9-NAT10 + AAV9-shMybbp1a n = 3. **p < 0.01 vs I/R + AAV9-NAT10 + AAV9-shNC. (H–I) Protein lysates obtained from Ischemic tissue in mice were immunoprecipitated with anti-P300 antibody or control IgG and then separated by 10% SDS-PAGE. Transferred membrane was immunoblotted with either anti-P300 or p53 antibody. (J) ChIP analysis of p53 binding to the promoter of SLC7A11. Cardiomyocytes were treated with NAT10 adenovirus and siMybbp1a and subjected to H/R at indicated time. ChIP was performed with p53 or IgG antibody. n = 3. *p < 0.05 vs IgG, $^{\#}$p < 0.05 vs H/R + Null + siNC, $^{\&\&}$p < 0.01 vs H/R + NAT10+siNC. Data are represented as mean ± SEM.

overexpressing hearts (Fig. 6A–B). Moreover, compared with that in the AAV9-shNC-treated group, Mybbp1a knockdown markedly ameliorated the cardiac function of I/R-exposed NAT10-overexpressing hearts (Fig. 6C–D). Moreover, the detrimental effects of NAT10 on cardiac ferroptosis after I/R were abolished by Mybbp1a knockdown, as indicated by increased GPX4 protein levels and decreased lipid peroxidation levels (Fig. 6E–G). Consistent with the in vivo results, knockdown of Mybbp1a abrogated the NAT10-induced decreases in viability and GPX4 protein levels and the increase lipid-ROS in H/R-exposed cardiomyocytes (Supplementary Figs. 7A–7C).

It has been reported that Mybbp1a induces cell death by enhancing p53 acetylation and transcriptional activation via P300 recruitment upon cellular stress [26]. We therefore hypothesized that NAT10-induced p53 activation occurred due to Mybbp1a/P300-mediated p53 acetylation. We then performed a coimmunoprecipitation assay to test this hypothesis. As shown in Fig. 6H, I/R increased the interaction between P300 and p53, and this interaction was markedly abrogated in AAV9-shNAT10 mice. In addition, NAT10 overexpression enhanced the binding of P300 to p53, and this interaction was inhibited by Mybbp1a knockdown (Fig. 6I). Silencing Mybbp1a significantly decreased the I/R- and H/R-induced upregulation of p53 and ac-k379-p53 protein expression (Supplementary Figs. 7D–7F). In addition, the NAT10-induced increases in p53 and ac-k379-p53 protein expression were reversed by Mybbp1a knockdown after I/R in vivo and in vitro (Supplementary Figs. 7G–7K). It has been shown that acetylated p53 inhibits cystine uptake and sensitizes cells to ferroptosis through the transcriptional inhibition of SLC7A11 expression [9]. Therefore, we performed a ChIP experiment to determine the effects of the NAT10/-Mybbp1 axis on the interaction of p53 with the SLC7A11 gene promoter region. As expected, overexpression of NAT10 promoted the binding of p53 to the SLC7A11 promoter in H/R-exposed cardiomyocytes, while silencing Mybbp1a reversed this effect (Fig. 6J). Furthermore, knockdown of NAT10 increased SLC7A11 expression in I/R-exposed hearts and H/R-exposed cardiomyocytes, whereas overexpression of NAT10

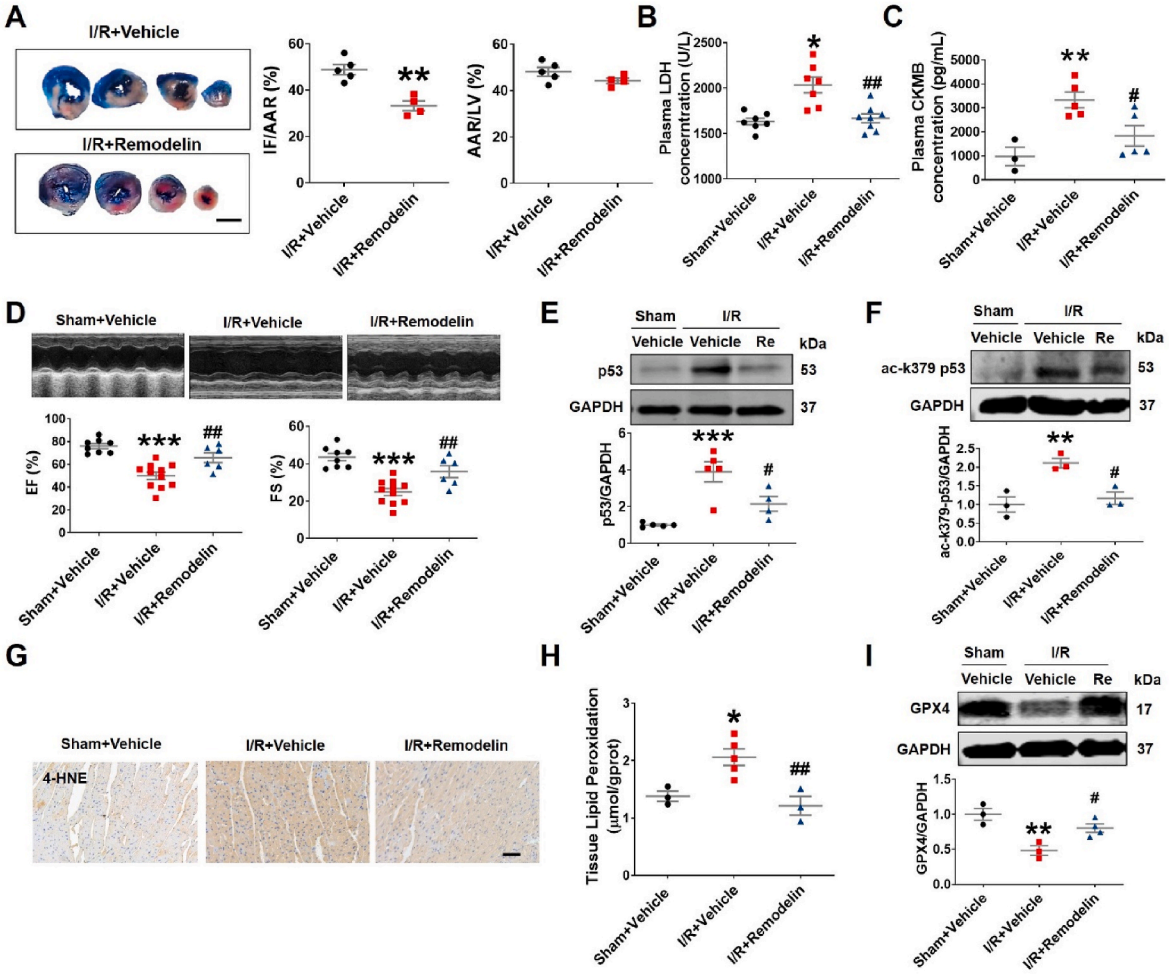

Fig. 7. Remodelin alleviated cardiac I/R injury.
(A) Infarct size of I/R hearts by Evans blue/TTC double staining (scale bar: 2 mm). IF: Infarct Area; AAR: Area at risk; LV: Left ventricle. I/R + Vehicle n = 5, I/R + Remodelin n = 4. **p < 0.01 vs I/R + Vehicle. (B) Plasma LDH was analyzed by a LDH assay kit. Sham + Vehicle n = 7, I/R + Vehicle n = 7, I/R + Remodelin n = 8. *p < 0.05 vs Sham + Vehicle, ##p < 0.01 vs I/R + Vehicle. (C) Plasma CKMB level was analyzed by Elisa assay. Sham + Vehicle n = 3, I/R + Vehicle n = 5, I/R + Remodelin n = 5. **p < 0.01 vs Sham + Vehicle, #p < 0.05 vs I/R + Vehicle. (D) Representative images of echocardiographs and statistics of ejection fraction (EF), fractional shortening (FS). Sham + Vehicle n = 8, I/R + Vehicle n = 11, I/R + Remodelin n = 6. ***p < 0.001 vs Sham + Vehicle, ##p < 0.01 vs I/R + Vehicle. (E) P53 protein level. Sham + Vehicle n = 5, I/R + Vehicle n = 5, I/R + Remodelin n = 4. ***p < 0.001 vs Sham + Vehicle, #p < 0.05 vs I/R + Vehicle. (F) Ac-k379-p53 protein level. Sham + Vehicle n = 3, I/R + Vehicle n = 3, I/R + Remodelin n = 3. **p < 0.01 vs Sham + Vehicle, #p < 0.05 vs I/R + Vehicle. (G) Immunohistochemical staining of 4-HNE in the heart tissues of mice 24 h after myocardial reperfusion injury (n = 3 per group, 4–5 fields per sample. Bar:50 μm). (H) Tissue Lipid peroxidation level was analyzed by Lipid-peroxidation assay kit. Sham + Vehicle n = 3, I/R + Vehicle n = 5, I/R + Remodelin n = 3. *p < 0.05 vs Sham + Vehicle, ##p < 0.01 vs I/R + Vehicle. (I) GPX4 protein level. Sham + Vehicle n = 3, I/R + Vehicle n = 3, I/R + Remodelin n = 3. **p < 0.01 vs Sham + Vehicle, #p < 0.05 vs I/R + Vehicle. Data are represented as mean ± SEM. (For interpretation of the references to colour in this figure legend, the reader is referred to the Web version of this article.)

had the opposite effect (Supplementary Figs. 8A–8D). In addition, knockdown of Mybbp1a suppressed the NAT10-or I/R-induced increase in SLC7A11 protein expression in vivo and in vitro (Supplementary Figs. 8E–8H). These results demonstrate that the detrimental effects of NAT10 on cardiac I/R injury were mediated by the Mybbp1a/p53 axis.

3.7. Remodelin alleviated cardiac I/R injury

These results suggest that NAT10 is a potential target for treating I/R. To further verify this hypothesis, we pretreated mice with Remodelin, which is a small molecule inhibitor of NAT10, to investigate whether it can ameliorate cardiac I/R injury. As expected, oral administration of Remodelin markedly reduced both I/R-induced increases in NAT10 mRNA and protein expression (Supplementary Figs. 9A–9B). However, Remodeling failed to alter the mRNA and protein levels of NAT10 in cardiomyocytes under physiological condition (Supplementary Figs. 9C–9D). Additionally, H/R-induced increase in NAT10 mRNA and protein expression in NMCMs was reversed by Remodelin (Supplementary Figs. 9C–9D). H/R-induced increase in Mybbp1a protein expression in NMCMs was reversed by Remodelin (Supplementary Fig. 9E). Notably, compared with vehicle-treated mice, Remodelin-treated mice had a reduced myocardial infarct size after I/R (Fig. 7A). I/R-induced LDH and CKMB release from I/R-exposed hearts was markedly suppressed by Remodelin (Fig. 7B–C). Echocardiography analysis revealed that I/R-induced cardiac dysfunction was greatly ameliorated after Remodelin treatment compared with vehicle treatment (Fig. 7D). At the molecular level, compared with the vehicle, Remodelin repressed the I/R-induced upregulation of p53 and Ac-k379-p53 protein expression (Fig. 7E–F). Furthermore, Remodelin treatment suppressed I/R-induced cardiac ferroptosis, as demonstrated by decreases in the accumulation of cardiac lipid peroxidation and the increase in GPX4 and SLC7A11 protein expression (Fig. 7G–I; Supplementary Fig. 8I). These results demonstrate that Remodelin alleviates cardiac ferroptosis and I/R injury.

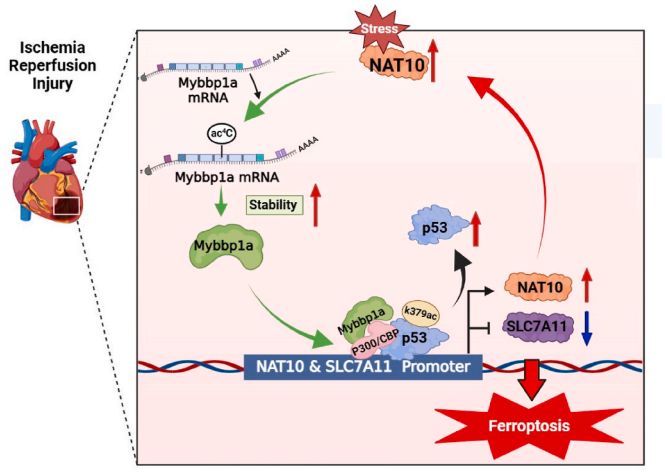

Fig. 8. Schematic illustration on the proposed mechanism of NAT10 on cardiac I/R injury. During cardiac I/R injury, the elevated expression of NAT10 enhances the stability of Mybbp1a through ac4C mdification, which in turn activateds p53 via P300-mediated acetylation, thereby repressing the transcription of the anti-ferroptotic gene SLC7A11. Meanwhile, p53 acts as a transcriptional activator to upregulate the expression of NAT10 after cardiac I/R. Based on these findings, a novel positive feedback regulatory circuit is proposed: I/R or H/R → NAT10 ↑→ Mybbp1a↑ → p53↑ → SLC7A11 ↓/ NAT10↑ → Cardiomyocytes ferroptosis → I/R or H/R injury↑ (Created with Biorender.com).

4. Discussion

Our study provided a number of new findings. (1) NAT10 mRNA and protein levels were significantly elevated in cardiomyocytes from I/R-exposed hearts; (2) P53 acted as a transcriptional activator to upregulate NAT10 expression in I/R-exposed hearts; (3) NAT10 deficiency alleviated while NAT10 overexpression exacerbated cardiomyocyte ferroptosis; (4) NAT10 caused the ac4C modification of Mybbp1a to increase its stability, thereby activating p53 via P300-mediated acetylation, which in turn induced the expression of the anti-ferroptotic gene SLC7A11; and (5) pharmacological inhibition of NAT10 via the inhibitor Remodelin protected against cardiac I/R injury. Taken together, these findings indicate that NAT10 forms a positive feedback loop with Mybbp1a/p53 to exacerbate cardiac I/R injury (Fig. 8).

During the course of this study, an article was published that reported the role of NAT10 in the heart [14]. These authors demonstrated that a PIWI-interacting RNA, termed HAAPIR, interacts with NAT10 to enhance its ac4C acetylation activity on the transcript of a proapoptotic protein, thus promoting cardiomyocyte apoptosis. However, whether NAT10 expression levels are altered in infarcted mouse myocardial tissues and H/R-exposed cardiomyocytes is still unknown. In comparison, we showed that the mRNA and protein levels of NAT10 were markedly upregulated in both mouse hearts exposed to I/R and a cellular model of H/R-induced oxidative stress, and these changes were accompanied by increased RNA ac4C levels. NAT10 is a nucleolar protein that translocates into the nucleoplasm upon exposure to different cellular stresses [27]. Liu et al. showed that the DNA damage-induced increase in NAT10 expression is absent in p53-deficient cells, suggested that the change in NAT10 expression depends on p53 [27]. It is well known that p53 functions as a transcription factor to activate and repress the transcription of many genes, including genes involved in ferroptosis, apoptosis, cell cycle arrest, and senescence, by binding to DNA promoters in a sequence-specific manner [28–32]. P53 activates its physiological antagonist MDM2 to form a negative feedback loop with MDM2 [33,34]. This evidence prompted us to consider the possibility that p53 may affect NAT10 expression in a transcription-dependent manner under I/R conditions. Consistent with these findings, our data demonstrated that overexpression of p53 increased while knockdown of p53 significantly decreased the mRNA and protein levels of NAT10 in I/R-exposed hearts and in H/R-exposed cardiomyocytes. Further studies showed that p53 acts as an upstream regulator to activate NAT10 transcription by binding specific DNA sequences during I/R injury.

A recent study demonstrated that cardiomyocyte apoptosis occurs mainly in the early phase, while ferroptosis occurs in the late phase, of I/R injury [3]. Inhibition of ferroptosis confers cardioprotective effects against cardiac I/R injury, especially in the late phase (after 4 h) after I/R. Although NAT10 has been shown to promote cardiomyocyte apoptosis upon oxidative stress [14], the role of NAT10 during cardiac I/R injury in vivo has yet to be determined. Our study identified NAT10 acts as a crucial regulator of cardiac I/R injury by regulating p53 stability and activity via gain- and loss-of-function strategies. More importantly, we found that NAT10 overexpression is sufficient to cause cardiomyocyte ferroptosis, which results in a slight decrease in cardiac function. Especially when the reperfusion time reaches 24 h or even longer, I/R-induced myocardial cell death mainly occurs via ferroptosis [3]. Our experimental results further confirmed that, when NAT10 was overexpressed, a ferroptosis inhibitor had superior cardioprotective effects compared with an apoptosis inhibitor. This finding suggested that NAT10 participates in I/R injury primarily by regulating ferroptosis. These results provide novel insights into the function of NAT10 in regulating multiple forms of cardiomyocyte death during I/R injury.

NAT10 and Mybbp1a are nucleolar proteins that translocate into the nucleoplasm upon cellular damage and contribute to nucleolar stress responses by regulating p53 [20,27]. For the first time, our study elucidated the regulatory role of NAT10 in Mybbp1a activation in cardiomyocytes exposed to I/R. We found that NAT10 markedly increased

the ac4C modification of Mybbp1a mRNA, which led to pronounced increases in Mybbp1a stability; thus, these findings provide a novel link in NAT10-Mybbp1a-p53 axis in terms of signal transduction from the nucleolus to the nucleoplasm in the context of I/R. In addition, in comparison with the study by Wang [14] et al., we identified Mybbp1a as a key target of NAT10-mediated ac4C modification that is involved in cardiomyocyte ferroptosis.

The acetylation of p53 at lysine residues in its CTD in response to DNA damage increases its stability by preventing the ubiquitination of the same lysine residues [35]. This acetylation of p53 is also crucial for its sequence-specific DNA binding activity and transcriptional activity [36].Mybbp1a has been shown to promote p53 tetramerization and recruit P300/CBP to enhance the acetylation of p53 in its CTD, thereby increasing the DNA-binding activity of p53 and promoting the transcription of target genes [22]. Knockdown of Mybbp1a suppressed the DNA damage agent-induced increase in p53 K382 acetylation and cell death in human cells [21].The acetylation of P53 in CTD is indispensable for promoting cells ferroptosis. Upon oxidative stress, the activated p53 has been shown to bind to the promoter region of the anti-ferroptotic SLC7A11 gene to repress its transcription, thereby sensitizing cells to ferroptosis by increasing accumulation of lipid peroxides [9]. The decreased level of p53 K382 acetylation or mutations in p53 lysine residues of CTD reduces the ability of p53 to repress SLC7A11 [11]. Consistent with these observations, we found that NAT10 overexpression promoted the interaction of P300 with p53, which was abrogated by silencing of Mybbp1a. Moreover, the level of p53 acetylation at K382 (corresponding to K379 in mice) was markedly increased in I/R-exposed hearts and H/R-exposed cardiomyocytes, and these effects were prevented by knockdown of NAT10 or Mybbp1a, which was accompanied by decreased expression of p53, Ac-p53-k379 and SLC7A11. Our study demonstrated that the upregulated NAT10 promoted cardiomyocytes ferroptosis by impairing the redox balances to increase lipid ROS levels and accumulation of lipid peroxidation via activating Mybbp1a/p53/SLC7A11 axis.

NAT10 is considered to be a lysine acetyltransferases (KAT) and functions as the writer of ac4C by transferring an acetyl group to proteins and RNAs via its substrate acetyl-CoA [37,38]. Remodelin was first identified as a small molecule inhibitor of the acetyltransferase activity of NAT10 and to improve the nuclear architecture of laminopathic cells [39]; however, the potential mechanism underlying the inhibitory effect of Remodelin on NAT10 is unclear. A biophysical study by Shrimp et al. showed that Remodelin fails to affect the NAT10-mediated RNA acetylation of cytidine [40]. In sharp contrast, a recent study predicted the structure of NAT10 and the potential sites at which Remodelin binds to NAT10 using molecular docking. This study indicated that Remodelin binds to NAT10 at the binding pocket of acetyl-CoA, thereby inhibiting the acetyltransferase activity of NAT10 and preventing the acetylation of both proteins and RNAs [41]. This is strongly supported by some studies showing that Remodelin inhibits ac4C RNA levels and NAT10 expression in human immunodeficiency virus and cancer [42–44]. Contrary to this consensus, a few studies have reported that NAT10 expression cannot be altered by Remodelin [45,46]. Our study showed that Remodelin markedly reduced the acetyltransferase activity of NAT10, which is necessary for catalyzing RNA acetylation, as indicated by reduced levels of ac4C in total RNA and reduced levels of ac4C in Mybbp1a mRNA in I/R-exposed hearts and H/R-exposed cardiomyocytes. In addition, we also found that Remodelin can reduce the mRNA and protein expression levels of NAT10 in I/R-exposed hearts and H/R-exposed cardiomyocytes, while this inhibitory effect on NAT10 expression was disappeared in the context of normoxia. The possible explanation for this is that Remodelin inhibits the enzymatic activity of NAT10, which in turn repressed the activation of positive feedback loop of NAT10/Mybbp1a/p53 axis in the mouse heart upon I/R, thereby suppressing the transcription of NAT10.

In conclusion, this study revealed that NAT10 is a central regulator of cardiomyocytes ferroptosis after cardiac I/R. We demonstrate that NAT10 increases the Mybbp1a stability via mediating ac4C modification, leading to transcriptional inhibition of SLC7A11 by inducing P300-mediated P53 acetylation and activation. Meanwhile, p53 transcriptionally upregulate the expression of NAT10, thereby forming a positive feedback loop with NAT10/Mybbp1a/SLC7A11 to exacerbate cardiac I/R injury. These findings suggest that targeting the p53/NAT10/Mybbp1a axis constitutes a new direction for treating cardiac I/R injury.

Funding

This work was supported by grants from the Natural Science Foundation of China [82273928, 82330011, U21A20339]; Youth Project of Scientific Research Institution of Heilongjiang Province [CZKYF2023-1-C047]; CAMS Innovation Fund for Medical Sciences (CIFMS) 2019-I2M-5–078.

CRediT authorship contribution statement

Zhezhe Qu: Data curation, Methodology, Project administration. **Xiaochen Pang:** Project administration. **Zhongting Mei:** Conceptualization. **Ying Li:** Conceptualization. **Yaozhi Zhang:** Conceptualization. **Chuanhao Huang:** Conceptualization. **Kuiwu Liu:** Conceptualization. **Shuting Yu:** Conceptualization. **Changhao Wang:** Conceptualization. **Zhiyong Sun:** Conceptualization. **Yingqi Liu:** Conceptualization. **Xin Li:** Conceptualization. **Yingqiong Jia:** Conceptualization. **Yuechao Dong:** Conceptualization. **Meixi Lu:** Conceptualization. **Tiantian Ju:** Conceptualization. **Fan Wu:** Conceptualization. **Min Huang:** Conceptualization. **Na Li:** Conceptualization. **Shunkang Dou:** Conceptualization. **Jianhao Jiang:** Conceptualization. **Xianhui Dong:** Conceptualization. **Yi Zhang:** Conceptualization. **Wanhong Li:** Conceptualization. **Baofeng Yang:** Conceptualization. **Weijie Du:** Funding acquisition, Writing – original draft, Writing – review & editing.

Declaration of competing interest

The authors declare that they have no competing interest.

Data availability

Data will be made available on request.

Appendix A. Supplementary data

Supplementary data to this article can be found online at https://doi.org/10.1016/j.redox.2024.103145.

References

[1] B. Geller, S. Sinha, N. Kapur, M. Bakitas, L. Balsam, J. Chikwe, et al., Escalating and de-escalating temporary mechanical circulatory support in cardiogenic shock: a scientific statement from the American heart association, Circulation 146 (2022) e50–e68.
[2] J.E. Tamis-Holland, H. Jneid, H.R. Reynolds, S. Agewall, E.S. Brilakis, T.M. Brown, et al., Contemporary diagnosis and management of patients with myocardial infarction in the absence of obstructive coronary artery disease: a scientific statement from the American heart association, Circulation 139 (2019) e891–e908.
[3] W. Cai, L. Liu, X. Shi, Y. Liu, J. Wang, X. Fang, et al., Alox15/15-HpETE aggravates myocardial ischemia-reperfusion injury by promoting cardiomyocyte ferroptosis, Circulation 147 (2023) 1444–1460.
[4] H. Xiao, M. Zhang, H. Wu, J. Wu, X. Hu, X. Pei, et al., CIRKIL exacerbates cardiac ischemia/reperfusion injury by interacting with Ku70, Circ. Res. 130 (2022) e3–e17.
[5] Y. Bei, D. Lu, C. Bär, S. Chatterjee, A. Costa, I. Riedel, et al., miR-486 attenuates cardiac ischemia/reperfusion injury and mediates the beneficial effect of exercise for myocardial protection, Mol. Ther. 30 (2022) 1675–1691.
[6] J. Lin, Q. Li, T. Jin, J. Wang, Y. Gong, Q. Lv, et al., Cardiomyocyte IL-1R2 protects heart from ischemia/reperfusion injury by attenuating IL-17RA-mediated cardiomyocyte apoptosis, Cell Death Dis. 13 (2022) 90.
[7] W. Flameng, M. Borgers, W. Daenen, G. Stalpaert, Ultrastructural and cytochemical correlates of myocardial protection by cardiac hypothermia in man, J. Thorac. Cardiovasc. Surg. 79 (1980) 413–424.

[8] S. Kumfu, J. Sripetchwandee, C. Thonusin, N. Sumneang, C. Maneechote, B. Arunsak, et al., Ferroptosis inhibitor improves cardiac function more effectively than inhibitors of apoptosis and necroptosis through cardiac mitochondrial protection in rats with iron-overloaded cardiomyopathy, Toxicol. Appl. Pharmacol. 479 (2023) 116727.
[9] L. Jiang, N. Kon, T. Li, S. Wang, T. Su, H. Hibshoosh, et al., Ferroptosis as a p53-mediated activity during tumour suppression, Nature 520 (2015) 57–62.
[10] S.J. Wang, D. Li, Y. Ou, L. Jiang, Y. Chen, Y. Zhao, et al., Acetylation is crucial for p53-mediated ferroptosis and tumor suppression, Cell Rep. 17 (2016) 366–373.
[11] H. Chen, X. Lin, X. Yi, X. Liu, R. Yu, W. Fan, et al., SIRT1-mediated p53 deacetylation inhibits ferroptosis and alleviates heat stress-induced lung epithelial cells injury, Int. J. Hyperther. 39 (2022) 977–986, the official journal of European Society for Hyperthermic Oncology, North American Hyperthermia Group.
[12] R. Kong, L. Zhang, L. Hu, Q. Peng, W. Han, X. Du, et al., hALP, a novel transcriptional U three protein (t-UTP), activates RNA polymerase I transcription by binding and acetylating the upstream binding factor (UBF), J. Biol. Chem. 286 (2011) 7139–7148.
[13] D. Arango, D. Sturgill, N. Alhusaini, A. Dillman, T. Sweet, G. Hanson, et al., Acetylation of cytidine in mRNA promotes translation efficiency, Cell 175 (2018), 1872-86.e24.
[14] K. Wang, L. Zhou, F. Liu, L. Lin, J. Ju, P. Tian, et al., PIWI-interacting RNA HAAPIR regulates cardiomyocyte death after myocardial infarction by promoting NAT10-mediated ac C acetylation of tfec mRNA, Adv. Sci. 9 (2022) e2106058.
[15] J. Shi, C. Yang, J. Zhang, K. Zhao, P. Li, C. Kong, et al., NAT10 is involved in cardiac remodeling through ac4C-mediated transcriptomic regulation, Circ. Res. 133 (2023) 989–1002.
[16] F. Tavner, R. Simpson, S. Tashiro, D. Favier, N. Jenkins, D. Gilbert, et al., Molecular cloning reveals that the p160 Myb-binding protein is a novel, predominantly nucleolar protein which may play a role in transactivation by Myb, Mol. Cell Biol. 18 (1998) 989–1002.
[17] M. Fan, J. Rhee, J. St-Pierre, C. Handschin, P. Puigserver, J. Lin, et al., Suppression of mitochondrial respiration through recruitment of p160 myb binding protein to PGC-1alpha: modulation by p38 MAPK, Gene Dev. 18 (2004) 278–289.
[18] V. Díaz, S. Mori, E. Longobardi, G. Menendez, C. Ferrai, R. Keough, et al., p160 Myb-binding protein interacts with Prep1 and inhibits its transcriptional activity, Mol. Cell Biol. 27 (2007) 7981–7990.
[19] Y. Hara, Y. Onishi, K. Oishi, K. Miyazaki, A. Fukamizu, N. Ishida, Molecular characterization of Mybbp1a as a co-repressor on the Period2 promoter, Nucleic Acids Res. 37 (2009) 1115–1126.
[20] T. Kuroda, A. Murayama, N. Katagiri, Y. Ohta, E. Fujita, H. Masumoto, et al., RNA content in the nucleolus alters p53 acetylation via MYBBP1A, EMBO J. 30 (2011) 1054–1066.
[21] T. Kumazawa, K. Nishimura, N. Katagiri, S. Hashimoto, Y. Hayashi, K. Kimura, Gradual reduction in rRNA transcription triggers p53 acetylation and apoptosis via MYBBP1A, Sci. Rep. 5 (2015) 10854.
[22] W. Ono, Y. Hayashi, W. Yokoyama, T. Kuroda, H. Kishimoto, I. Ito, et al., The nucleolar protein Myb-binding protein 1A (MYBBP1A) enhances p53 tetramerization and acetylation in response to nucleolar disruption, J. Biol. Chem. 289 (2014) 4928–4940.
[23] M. Guo, Y. Zhu, Y. Shi, X. Meng, X. Dong, H. Zhang, et al., Inhibition of ferroptosis promotes retina ganglion cell survival in experimental optic neuropathies, Redox Biol. 58 (2022) 102541.
[24] W. Cai, L. Liu, X. Shi, Y. Liu, J. Wang, X. Fang, et al., Alox15/15-HpETE aggravates myocardial ischemia-reperfusion injury by promoting cardiomyocyte ferroptosis, Circulation 147 (2023) 1444–1460.
[25] R. Wei, X. Cui, J. Min, Z. Lin, Y. Zhou, M. Guo, et al., NAT10 promotes cell proliferation by acetylating CEP170 mRNA to enhance translation efficiency in multiple myeloma, Acta Pharm. Sin. B 12 (2022) 3313–3325.
[26] K. Akaogi, W. Ono, Y. Hayashi, H. Kishimoto, J. Yanagisawa, MYBBP1A suppresses breast cancer tumorigenesis by enhancing the p53 dependent anoikis, BMC Cancer 13 (2013) 65.
[27] X. Liu, Y. Tan, C. Zhang, Y. Zhang, L. Zhang, P. Ren, et al., NAT10 regulates p53 activation through acetylating p53 at K120 and ubiquitinating Mdm2, EMBO Rep. 17 (2016) 349–366.
[28] A. Boutelle, L. Attardi, p53 and tumor suppression: it takes a network, Trends Cell Biol. 31 (2021) 298–310.
[29] Y. Liu, W. Gu, p53 in ferroptosis regulation: the new weapon for the old guardian, Cell Death Differ. 29 (2022) 895–910.
[30] P. Barnes, J. Baker, L. Donnelly, Cellular senescence as a mechanism and target in chronic lung diseases, Am. J. Respir. Crit. Care Med. 200 (2019) 556–564.
[31] K. Engeland, Cell cycle regulation: p53-p21-RB signaling, Cell Death Differ. 29 (2022) 946–960.
[32] C. Liu, Y. Zhang, R. Li, L. Zhou, T. An, R. Zhang, et al., LncRNA CAIF inhibits autophagy and attenuates myocardial infarction by blocking p53-mediated myocardin transcription, Nat. Commun. 9 (2018) 29.
[33] A. Thomas, E. White, Suppression of the p300-dependent mdm2 negative-feedback loop induces the p53 apoptotic function, Gene Dev. 12 (1998) 1975–1985.
[34] F.J. Stott, S. Bates, M.C. James, B.B. McConnell, M. Starborg, S. Brookes, et al., The alternative product from the human CDKN2A locus, p14(ARF), participates in a regulatory feedback loop with p53 and MDM2, EMBO J. 17 (1998) 5001–5014.
[35] A. Ito, C. Lai, X. Zhao, S. Saito, M. Hamilton, E. Appella, et al., p300/CBP-mediated p53 acetylation is commonly induced by p53-activating agents and inhibited by MDM2, EMBO J. 20 (2001) 1331–1340.
[36] J. Luo, M. Li, Y. Tang, M. Laszkowska, R. Roeder, W. Gu, Acetylation of p53 augments its site-specific DNA binding both in vitro and in vivo, Proc. Natl. Acad. Sci. U.S.A. 101 (2004) 2259–2264.
[37] S. Ito, S. Horikawa, T. Suzuki, H. Kawauchi, Y. Tanaka, T. Suzuki, et al., Human NAT10 is an ATP-dependent RNA acetyltransferase responsible for N4-acetylcytidine formation in 18 S ribosomal RNA (rRNA), J. Biol. Chem. 289 (2014) 35724–35730.
[38] D. Montgomery, J. Garlick, R. Kulkarni, S. Kennedy, A. Allali-Hassani, Y. Kuo, et al., Global profiling of acetyltransferase feedback regulation, J. Am. Chem. Soc. 138 (2016) 6388–6391.
[39] D. Larrieu, S. Britton, M. Demir, R. Rodriguez, S. Jackson, Chemical inhibition of NAT10 corrects defects of laminopathic cells, Science (New York, NY) 344 (2014) 527–532.
[40] J. Shrimp, Y. Jing, S. Gamage, K. Nelson, J. Han, K. Bryson, et al., Remodelin is a cryptic assay interference chemotype that does not inhibit NAT10-dependent cytidine acetylation, ACS Med. Chem. Lett. 12 (2021) 887–892.
[41] M. Dalhat, H. Altayb, M. Khan, H. Choudhry, Structural insights of human N-acetyltransferase 10 and identification of its potential novel inhibitors, Sci. Rep. 11 (2021) 6051.
[42] G. Balmus, D. Larrieu, A. Barros, C. Collins, M. Abrudan, M. Demir, et al., Targeting of NAT10 enhances healthspan in a mouse model of human accelerated aging syndrome, Nat. Commun. 9 (2018) 1700.
[43] K. Tsai, A. Jaguva Vasudevan, C. Martinez Campos, A. Emery, R. Swanstrom, B. Cullen, Acetylation of cytidine residues boosts HIV-1 gene expression by increasing viral RNA stability, Cell Host Microbe 28 (2020), 306-12.e6.
[44] J. Wu, H. Zhu, J. Wu, W. Chen, X. Guan, Inhibition of N-acetyltransferase 10 using remodelin attenuates doxorubicin resistance by reversing the epithelial-mesenchymal transition in breast cancer, Am. J. Tourism Res. 10 (2018) 256–264.
[45] W. Yang, H. Li, Y. Wu, R. Mi, W. Liu, X. Shen, et al., ac4C acetylation of RUNX2 catalyzed by NAT10 spurs osteogenesis of BMSCs and prevents ovariectomy-induced bone loss, Mol. Ther. Nucleic Acids 26 (2021) 135–147.
[46] N. Ma, H. Liu, Y. Wu, M. Yao, B. Zhang, NInhibition of -acetyltransferase 10 suppresses the progression of prostate cancer through regulation of DNA replication, Int. J. Mol. Sci. 23 (2022).